Kinetic Parameter Estimation of HDPE Slurry Process from Molecular Weight Distribution: Estimability Analysis and Multistep Methodology

Chen Zhang, Zhijiang Shao, and Xi Chen
State Key Laboratory of Industrial Control Technology, Dept. of Control Science and Engineering, Zhejiang University, Hangzhou, Zhejiang 310027 P.R. China

Zhen Yao and Xueping Gu
State Key Laboratory of Chemical Engineering, Dept. of Chemical and Biological Engineering, Zhejiang University, Hangzhou, Zhejiang 310027 P.R. China

Lorenz T. Biegler
Dept. of Chemical Engineering, Carnegie Mellon University, Pittsburgh, PA 15213

DOI 10.1002/aic.14527
Published online June 24, 2014 in Wiley Online Library (wileyonlinelibrary.com)

This study addresses kinetic parameter estimation for a high-density polyethylene (HDPE) slurry process based on fitting molecular weight distributions (MWDs). From the process model, we conduct an estimability analysis by assessing the relative sensitivity between output variables and kinetic parameters as well as confidence intervals. This determines which parameters can be estimated. Conversely, a major challenge remains with the solution of an ill-conditioned parameter estimation problem with MWD as the output variable. To overcome the convergence difficulties with the associated problem, we develop a novel multistep methodology where we first obtain MWD parameters by matching to data and then estimate kinetic parameters by matching to the regressed MWD parameters. Computational results and eigenvalue analysis show this multistep methodology separates an ill-conditioned problem into two well-conditioned subproblems. Moreover, we consider simulation-based and industrial HDPE case studies. These results demonstrate the applicability, potential, and efficiency of this solution procedure. © 2014 American Institute of Chemical Engineers *AIChE J*, 60: 3442–3459, 2014

Keywords: kinetic parameter estimation, molecular weight distribution, estimability analysis, multistep methodology, eigenvalue analysis

Introduction

High-density polyethylene (HDPE) is one of the most widely used synthetic commodity polymers in the film, pipe, and container industries. Continuous slurry polymerization with heterogeneous Ziegler–Natta catalysts is a popular process for HDPE production, in which polymer grows at the active sites on the catalyst until chain transfer occurs, thus forming dead polymer chains.[1] The molecular weight distribution (MWD) is at the core in establishing key quality indices for polymers as their extreme versatility[2] derives from the way the monomer molecules are connected to form the polymer chains. Specifically, toughness, hardness, stiffness, strength, and viscoelasticity are among the properties dependent on MWD.[3] Once MWD is determined, other quality indices, such as polydispersity index (PDI), number average molecular weight (Mn), and weight average molecular weight (Mw), are also determined.

Mathematical modeling is a powerful tool for the development of process understanding and advanced reactor technology in the polymer industry.[4] Kinetic parameter estimation plays a central role in the systematic model development. Generally, the kinetic parameters are estimated with multiple sets of process data, including the operating conditions and product qualities. In fact, determining the kinetic parameters could be the most complicated and time-consuming task for the successful development of the process model. It is expected that the obtained kinetic parameters show a very good description of the plant data used in the estimation process, and also allow a robust and accurate prediction of the process performance under a wide range of operating conditions.

Research efforts on parameter estimation theory and methods have been made recently to aid parameter estimation in mathematical models for polymerization processes. Kou et al.[5] considered a rigorous model for gas-phase ethylene homopolymerization using a supported metallocene catalyst. Estimability analysis techniques were applied to aid in the parameter estimation. Matos et al.[6] developed a technique for determining kinetic parameters of ethylene/propylene

Correspondence concerning this article should be addressed to X. Chen at xichen@iipc.zju.edu.cn or L. T. Biegler at lb01@andrew.cmu.edu.

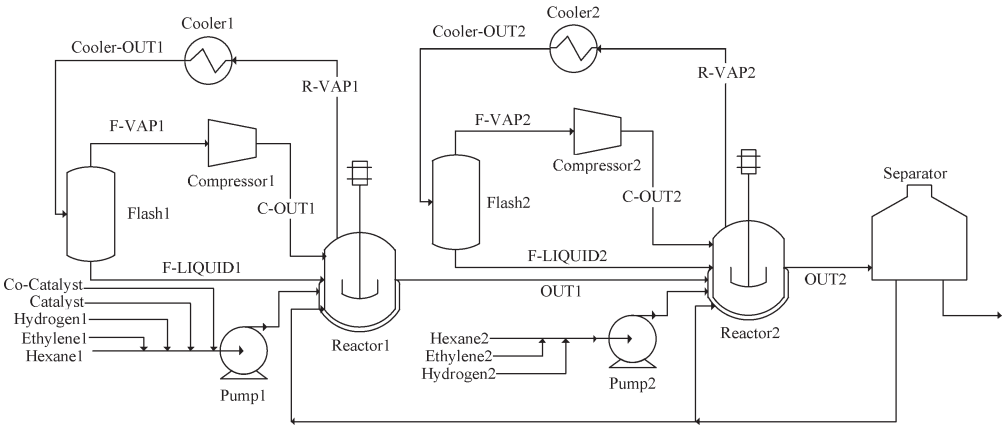

Figure 1. Flow sheet of HDPE slurry process in series.

copolymerization during the synthesis of high impact polypropylene in a train of cascade reactors. Nonlinear least-squares estimation was used for parameter estimation in their submodels. Sirohi and Choi[7] investigated two different online parameter estimation schemes to estimate key kinetic parameters of transition metal-catalyzed olefin polymerization. Lo and Ray[8] developed a kinetic model for ethylene polymerization over nickel diimine catalysts. Experimental data from the literature were used to fit the model kinetic parameters. For gas-phase free-radical copolymerization of ethylene in tubular reactors, Zavala and Biegler[9] considered efficient strategies to enable the solution of challenging estimation problems including multiple data and large parameters sets. Embiruçu et al.[10] developed and applied a methodology to allow estimation of kinetic parameters for industrial continuous ethylene/1-butene polymerizations using soluble Ziegler–Natta catalysts. The parameter estimation procedure was formulated as a nonlinear optimization procedure subject to hard and soft constraints. Li et al.[11] proposed a hierarchical extended Kalman filter design to estimate unmeasured state variables and key kinetic parameters of a continuous ethylene-propylene-diene polymer reactor. Khare et al.[12,13] developed a manually implemented iterative parameter estimation methodology, which adjusted parameters manually to ensure that they could match the data for each grade. Thompson et al.,[14] Yao et al.,[15] and Li et al.[16] developed estimability analysis techniques that enabled automated estimation of parameters in complex polymerization models, using limited experimental data. A parametric sensitivity matrix was used to provide information about the influence of each kinetic parameter on both model predictions and their correlation with each other. Conversely, most of these studies[7–13,15–20] did not attempt to estimate the kinetic parameters of polymerization processes from MWDs, due to the complexity of MWD modeling and calculation. As a result, these approaches need large amounts of plant data to estimate parameters and generate models. Otherwise, insufficient data lead to parameters with large confidence regions and nonrobust model predictions.[6]

This study addresses the kinetic parameter estimation for HDPE slurry process with specified MWD measurements. We first develop a comprehensive equation-oriented (EO) model and apply an estimability analysis based on available MWD information. A systematic approach for the selection of estimable parameters is proposed. We then develop a novel multistep methodology to estimate the kinetic parameters by solving three nonlinear programming (NLP) optimization problems sequentially. Intermediate variables that relate directly to the target MWDs are introduced and estimated as well. The results on three large-scale case studies show the advantages of this methodology on the estimation accuracy, ease of convergence, and computational effort.

Model Development

Figure 1 illustrates the flow sheet of an industrial HDPE slurry process[12] on the basis of CX polymerization technology from Mitsui Chemicals. A Ziegler–Natta catalyst, with titanium tetrachloride ($TiCl_4$) as the catalyst and triethyl aluminum ($Al(C_2H_5)_3$) as the cocatalyst, is used. The process consists of two continuous stirred-tank reactors (CSTRs) in series, together with other units including flash drums, coolers, compressors, and pumps. Ethylene (monomer), hydrogen (chain transfer agent), *n*-hexane (diluent), and the Ziegler–Natta catalyst system are fed continuously to the first CSTR. The product stream leaving the first reactor is fed into the second reactor together with fresh ethylene, hydrogen, and hexane. The vapor streams leaving reactors, which contain ethylene, hydrogen, and hexane are recycled to the feed streams through coolers, flash drums, and compressors to achieve high monomer conversion. The highly concentrated slurry product leaving the second reactor is fed to a centrifugal separator that removes unreacted monomer and diluent from the polymer solids. The diluent is then completely recovered while the polymer product is dried and pelletized.

A complete EO model is established for the slurry process. The perturbed-chain statistical associating fluid theory equation of state (PC-SAFT EOS)[21] is used to model the thermodynamic properties. As this complex EOS model is difficult to solve by the EO approach, a set of surrogate kriging[22] models, based on the data generated from PC-SAFT EOS, was applied from our previous work.[23] Moreover, unit models with additional phase equilibrium, mass and energy equations were incorporated from our previous work,[24] as listed in Appendix A. The resulting kinetics and MWD models are presented next.

Homopolymerization kinetics

The kinetic mechanism[24] of ethylene homopolymerization with Ziegler–Natta catalyst system is summarized in Table

1, where C_P is a potential active site of catalyst $TiCl_4$, A is cocatalyst $Al(C_2H_5)_3$, M is monomer, H_2 is hydrogen, P_0 is an active site, C_d is a deactivated site, D_n is a dead polymer of chain length n, P_n is a living polymer chain of length n, j represents the index of active sites, and k_{aA}, k_i, k_p, k_{tM}, k_{tH}, k_{tA}, k_t, k_d are the kinetic rate constants of different reactions, respectively. The Arrhenius equation is used to determine the kinetic rate constant k

$$k = k^0 \exp\left[-\frac{E^a}{\bar{R}}\left(\frac{1}{T}-\frac{1}{T_{ref}}\right)\right] \tag{1}$$

where k^0 is the pre-exponential kinetic rate constant, E^a is the activation energy, $\bar{R}$ is the universal gas constant, T is the reaction temperature, and T_{ref} is the reference temperature.

Heterogeneous Ziegler–Natta catalysts possess multiple active sites, even on the same catalyst particle; the traditional approach to model their multiplicity is to assume a finite number of different site types with distinct kinetic rate constants. We also assume that one type of active site cannot turn into a different type. Usually, the number of active sites can be determined by the deconvolution of polymer distributions. Soares and Hamielec[25] compared two numerical methods for the deconvolution of polypropylene chain length distribution (CLD) to obtain an adequate number of active sites. Recently, they[26] described an integrated deconvolution estimation model, in which the MWD of polyolefins was deconvoluted to determine the minimum number of site types by minimizing the sum of squares of the differences between experimental and predicted MWDs until the fit cannot be improved any further. Similarly, by deconvoluting the measured distribution of a specimen, Hakim and Mobalegh[27] found that five or six site types should be considered for HDPE slurry process using Ziegler–Natta catalyst. In our model, the number of active sites is set to 5 based on the knowledge and experience of technologists. As seen from our previous work[24] and the numerical results below, using this number of sites fits the data well.

According to the mechanism in Table 1, we define the following pseudokinetic rate constant of transfer and deactivation

$$K_{TD}(j) = k_{tM}(j)[M]_L^R + k_{tH}(j)([H_2]_L^R)^{0.5} + k_{tA}(j)[A] + k_t(j) + k_d(j) \tag{2}$$

where [.] denotes the concentration of the inside component in the reactor, the subscript L denotes the liquid phase, and the superscript R denotes the reactor. For living chains of length $n=1$, the net reaction rate takes the form

$$\begin{aligned} r_{P_1(j)} = {} & k_i(j)[M]_L^R[P_0(j)] + k_{tM}(j)[M]_L^R Y^0(j) \\ & - k_p(j)[M]_L^R[P_1(j)] - K_{TD}(j)[P_1(j)] \end{aligned} \tag{3}$$

where $Y^0(j) = \sum_{n=1}^{\infty}[P_n(j)]$ is the sum of living chain concentrations.

For living chains of length $n \geq 2$, the net reaction rate takes the form

$$r_{P_n(j)} = \left(k_p(j)[M]_L^R([P_{n-1}(j)] - [P_n(j)])\right) - K_{TD}(j)[P_n(j)] \tag{4}$$

Similarly, the net reaction rate for dead chains of length $n = 1$ is given by

$$r_{D_1(j)} = K_{TD}(j)[P_1(j)] - k_{tM}[M]_L^R[P_1(j)] \tag{5}$$

Table 1. Kinetic Mechanism of Homopolymerization

Reaction Types	Descriptions
Activation	$C_p(j) + A \xrightarrow{k_{aA}(j)} P_0(j)$
Initiation	$P_0(j) + M \xrightarrow{k_i(j)} P_1(j)$
Propagation	$P_n(j) + M \xrightarrow{k_p(j)} P_{n+1}(j)$
Transfer to monomer	$P_n(j) + M \xrightarrow{k_{tM}(j)} P_1(j) + D_n(j)$
Transfer to hydrogen	$P_n(j) + H_2 \xrightarrow{k_{tH}(j)} P_0(j) + D_n(j)$
Transfer to cocatalyst	$P_n(j) + A \xrightarrow{k_{tA}(j)} P_0(j) + D_n(j)$
Transfer β-hydride	$P_n(j) \xrightarrow{k_t(j)} P_0(j) + D_n(j)$
Deactivation	$P_n(j) \xrightarrow{k_d(j)} C_d(j) + D_n(j)$
	$P_0(j) \xrightarrow{k_d(j)} C_d(j)$

and the net reaction rate for dead chains of length $n \geq 2$ becomes

$$r_{D_n(j)} = K_{TD}(j)[P_n(j)] \tag{6}$$

The net reaction rates for potentially active, active, and deactivated sites of catalyst can be calculated as follows

$$r_{C_p(j)} = -k_{aA}(j)[A]\left[C_p(j)\right] \tag{7}$$

$$\begin{aligned} r_{P_0(j)} = {} & -k_i(j)[M]_L^R[P_0(j)] - k_d(j)[P_0(j)] + k_{aA}(j)[A]\left[C_p(j)\right] \\ & + \left(k_{tH}(j)([H_2]_L^R)^{0.5} + k_{tA}(j)[A] + k_t(j)\right)Y^0(j) \end{aligned} \tag{8}$$

$$r_{C_d(j)} = k_d(j)\left([P_0(j)] + Y^0(j)\right) \tag{9}$$

For chain lengths with $n=1, 2, 3, \ldots, n_{max}$, the above equations can be solved to obtain the complete CLD with n_{max} is the maximum chain length. However, for high molecular weight polymers like HDPE, where n_{max} is 10^5 or more, the resulting system leads to a prohibitive number of equations and computational cost. Instead, the method of moments,[28,29] calculating the leading moments of the CLD with considerably less effort, is used to describe the mass balance of the polymer components. The rth moment of a generic distribution $f(x)$ is defined as

$$\mu^r = \sum_{x=1}^{\infty} x^r f(x) \tag{10}$$

so that the rth moments of living and dead polymer at the jth active site are given by

$$Y^r(j) = \sum_{n=1}^{\infty} n^r[P_n(j)] \tag{11}$$

$$X^r(j) = \sum_{n=2}^{\infty} n^r[D_n(j)] \tag{12}$$

For the zeroth moments of CLD of the living and dead polymer chains, the equations are derived by substituting the corresponding net reaction rates into the moment expressions

$$r_{Y^0(j)} = k_i(j)[M]_L^R[P_0(j)] + k_{tM}(j)[M]_L^R Y^0(j) - K_{TD}(j)Y^0(j) \tag{13}$$

$$r_{X^0(j)} = K_{TD}(j) Y^0(j) - k_{tM} [M]_L^R [P_1(j)] \quad (14)$$

For the first and second moments of CLD of the living and dead polymer chains, the net reaction rates are given by

$$r_{Y^1(j)} = k_i(j)[M]_L^R[P_0(j)] + k_p(j)[M]_L^R Y^0(j) + k_{tM}(j)[M]_L^R Y^0(j) - K_{TD}(j) Y^1(j) \quad (15)$$

$$r_{X^1(j)} = K_{TD}(j) Y^1(j) - k_{tM}[M]_L^R [P_1(j)] \quad (16)$$

$$r_{Y^2(j)} = k_i(j)[M]_L^R[P_0(j)] + k_{tM}(j)[M]_L^R Y^0(j) + k_p(j)[M]_L^R (2Y^1(j) + Y^0(j)) - K_{TD}(j) Y^2(j) \quad (17)$$

$$r_{X^2(j)} = K_{TD}(j) Y^2(j) - k_{tM}[M]_L^R [P_1(j)] \quad (18)$$

Typically, the zeroth, first, and the second moments are sufficient for the computation of common polymer properties like Mn, Mw, and PDI.

MWD calculation

In the steady-state slurry process, the CLD for HDPE polymerization at site j is given by a single-parameter equation, Flory's most probable distribution[30]

$$\tau_j = \frac{K_{TD}(j)}{K_P(j)} = \frac{k_{tM}(j)[M]_L^R + k_{tH}(j)([H_2]_L^R)^{0.5} + k_{tA}(j)[A] + k_t(j) + k_d(j)}{k_p(j)[M]_L^R} \quad (19)$$

$$\mathrm{cld}_j = n\tau_j^2/(1+\tau_j)^{n+1}, \quad n = 1, 2, 3, ..., n_{max} \quad (20)$$

where cld_j is the weight CLD of the polymer chains with length n, $n = 1, 2, 3, \ldots, n_{max}$, τ_j is the ratio of all the chain transfer rates to the propagation rate. The following transformations[31] convert CLD to MWD on the logarithmic scale, where mw is the molecular weight of ethylene, and mwd_j is the weight distribution at the jth active site on the logarithmic scale of molecular weight

$$\mathrm{mwd}_j = \ln 10 \times (\mathrm{mw} \times n)^2 \left(\frac{\tau_j}{\mathrm{mw}}\right)^2 \left(\frac{1}{1+\tau_j}\right)^{n+1}, \quad n = 1, 2, 3, ..., n_{max} \quad (21)$$

The entire distribution of the molecular weight for one reactor, $\overline{\mathrm{mwd}}$, can be obtained using the weighted superposition of Flory's distribution from each site

$$\overline{\mathrm{mwd}} = \sum_{j=1}^{Ns} \mathrm{mwd}_j \mathrm{mf}_j \quad (22)$$

where mf_j is the mole fraction of the polymer produced at site j.

$$\mathrm{mf}_j = \frac{Y^1(j) + X^1(j)}{\sum_{k=1}^{Ns} \left(Y^1(k) + X^1(k)\right)} \quad (23)$$

In the series configuration, the MWD of the final product leaving the second reactor is a combination of the two distributions in each reactor shown as follows

$$\mathrm{MWD} = \frac{m_1 \overline{\mathrm{mwd1}} + m_2 \overline{\mathrm{mwd2}}}{m_1 + m_2} \quad (24)$$

where MWD is the MWD of the final product. $\overline{\mathrm{mwd1}}$ and $\overline{\mathrm{mwd2}}$ are the distribution of the first and second reactors, respectively. m_1 and m_2 are the polymer masses of the first and second reactors, respectively, which can be calculated from the moment models. The complete steady-state process model, including kinetic mechanism, thermodynamics, MWD calculation, and mass and energy balance of all unit models, contains over 10,000 variables and equations.

Estimability Analysis

In a standard estimation problem, kinetic parameters are estimated by minimizing the deviation between the predicted and measured values of a set of output variables, with a weighted least-squares function selected as the objective. This problem includes multiple data sets that describe different operating conditions.[9] The set of output variables s corresponds to polymer properties, such as PDI, Mn, Mw, MWD, and the parameter estimation problem, with weighted least squares, can be stated as

$$\min_\theta E(\theta) = \sum_{l=1}^{N_C} \sum_{i=1}^{N_V} w_{i,l} (s(i,l)_{cal} - s(i,l)_{tar})^2$$
$$\text{s.t.} \quad G_{i,l}(s(i,l)_{cal}, \theta) = 0$$
$$i = 1, ..., N_V, l = 1, ..., N_C \quad (25)$$

where $E(\theta)$ is the objective function with the estimated parameter vector θ. N_C is the number of sets of steady-state operating conditions, N_V is the number of output variables under one set of operating conditions. $s(i,l)_{cal}$ and $s(i,l)_{tar}$ are the values of the i th calculated (predicted) and target (measured) output variable under the l th set of reactor operating conditions, respectively. $w_{i,l}$ is the corresponding weighting factor. Finally, the model equations $G_{i,l}$ relate the calculated outputs $s(i,l)_{cal}$ to θ, for the l th set of reactor operating conditions. Estimability analysis is used to determine the output variables and estimated parameters that provide a well-posed solution to (25).

Selection of output variables

Scalar measurements of polymer indices such as PDI, Mn, and Mw could be used as output variables. However, if one scalar property like Mw is used, we only have N_C data points from the outputs in (25). The maximum number of types of kinetic parameters we can estimate from one scalar property is $[N_C/N_S]$, where N_S is the number of types of active sites and $\lfloor . \rfloor$ rounds the argument down to the nearest integer. Conversely, MWD information is determined by two groups of parameters, τ_j and mf_j defined in Eqs. 19 and 23. As the sum of mf_j equals 1, there are $(2^* N_S - 1)$ independent parameters that determine one MWD profile. Under N_C sets of operating conditions, there are N_C *$(2^* N_S - 1)$ independent parameters and the maximum number of types of kinetic parameters we can estimate is $[N_C * (2 - 1/N_S)]$. Hence, with the same number of data sets, MWDs can be used to estimate many more kinetic parameters. For example, when $N_C = N_S = 5$, the maximum numbers of types of estimable kinetic parameters with one scalar property and MWD are 1 and 9, respectively. This characteristic of MWD means we could estimate kinetic parameters from limited data and obtain more reliable results. Hence, kinetic parameters will be estimated here from MWDs. These items comprise an NLP with a minimization objective function and constraint functions imposed by the process model equations

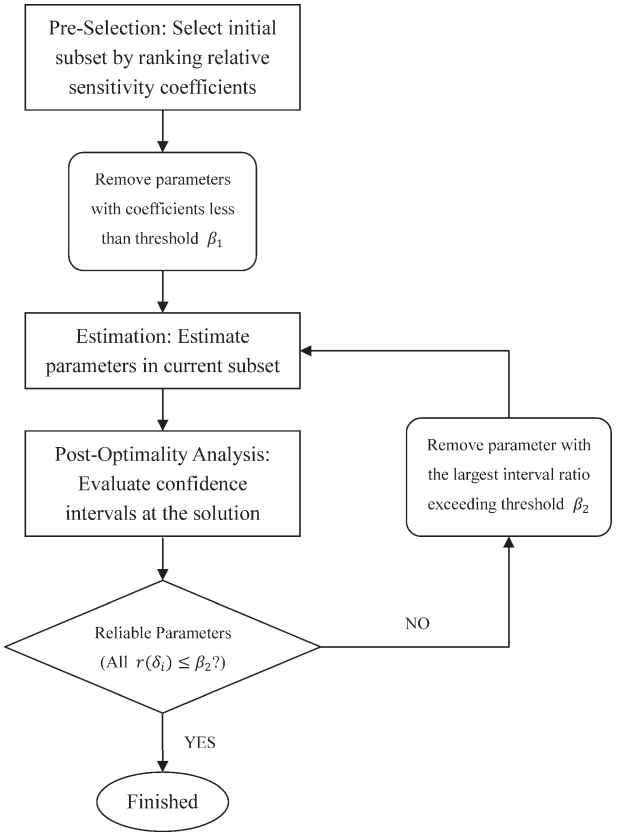

Figure 2. Flowchart of the estimated parameter selection approach.

$$\min_{\theta} \sum_{l=1}^{N_C}\sum_{m=1}^{N_P}\left[\overline{\text{mwd}}\,(l)_{\text{cal}}^{m}-\overline{\text{mwd}}\,(l)_{\text{tar}}^{m}\right]^2$$
$$\text{s.t.}\quad g_l\left(\overline{\text{mwd}}\,(l)_{\text{cal}},\theta\right)=0 \qquad (26)$$
$$l=1,\ldots,N_C$$

where $\overline{\text{mwd}}\,(l)_{\text{cal}}^{m}$ and $\overline{\text{mwd}}\,(l)_{\text{tar}}^{m}$ are the values of a sampling point m on the calculated and target MWDs under the l th set of reactor operating conditions, respectively. N_P is the number of sampling points comprising the curve, set to 100 by our experience. Because MWD is the only output variable, all weighting factors are set to 1. The equality constraint g_l relates $\overline{\text{mwd}}\,(l)_{\text{cal}}^{m}$ to the parameter vector θ, for the l th set of reactor operating conditions. This constraint includes the kriging model of thermodynamic properties, population balance, the method of moments and distribution in the reactors, and the quantitative behavior of other unit models.

Selection of estimated parameters

It should be mentioned that all of these kinetic parameters in Table 1 may not be readily estimated from MWD data sets. Obtaining a subset of estimable parameters and evaluating their reliability is an important task in parameter estimation.[32] Here, an approach for parameter selection and evaluation is proposed to determine which kinetic parameters can be estimated. The flowchart of the parameter selection approach is presented in Figure 2. In this approach, three steps (pre-selection, estimation, and post-optimality analysis) are applied. The basic idea is to remove parameters with small sensitivity coefficients and large confidence intervals from the estimable parameter subset. Pre-selection and Post-optimality analysis are discussed below. Estimation follows in the next section.

Pre-Selection. In the pre-selection step, sensitivity coefficients, that is, partial derivatives of the output variables with respect to the parameters are used to initially determine which kinetic parameters can be estimated. We rank the parameters based on the corresponding magnitudes of the coefficients. Parameters with coefficients less than a threshold are removed from the estimable subset and set to their literature values. Here, the threshold for the coefficients β_1 is set to two orders of magnitude.

The sensitivities of $\overline{\text{mwd}}$ with respect to $k(j)$ could be obtained by chain-ruling the derivatives of the intermediate quantities (mwd_j, mf_j, $X^1(j)$, $Y^1(j)$) from Eqs. 21–23. However, we do not use the sensitivities of $\overline{\text{mwd}}$ ($\partial\overline{\text{mwd}}/\partial k(j)$) directly. Instead, we use the derivatives of τ_j with respect to $k(j)$ to rank the kinetic parameters. Here, the relative sensitivity coefficient $\text{rsc}(k(j))$ is calculated, which changes τ_j and $k(j)$ to logarithmic form

$$\text{rsc}\,(k(j))=\frac{\partial \ln \tau(j)}{\partial \ln k(j)}=\frac{k(j)}{\tau(j)}\times\frac{\partial \tau(j)}{\partial k(j)} \qquad (27)$$

This coefficient compensates for different parameter scales and provides a more objective and meaningful comparison.

For this HDPE slurry process, we select the initial estimable subset based on parameter sensitivity coefficients at their literature values specified from our previous work.[24] The literature values of all the pre-exponential kinetic rate constants and the activation energies are listed in Tables 2 and 3, respectively. The corresponding coefficients are presented in Table 4. By examining the magnitudes of each coefficient in the table, we can rank the relative influence of different kinetic parameters. Here, the largest coefficient value is 10^0, so parameters with coefficients less than the threshold $\beta_1 = 10^{-2}$ are removed from the subset and set to their literature values. The large magnitudes (10^0) of the columns of k_p and k_{tH} indicate these kinetic parameters have a significant influence on the output variables while other kinetic parameters may not be estimated accurately due to their small influence (with magnitudes: $10^{-3}-10^{-8}$). Moreover, from the perspective of chemical technologists, it is known that k_p and k_{tH} have a dominant influence; the propagation reaction mainly determines the

Table 2. Literature Data of Pre-Exponential Kinetic Rate Constants in Homopolymerization

Reaction Types	Units	Site1	Site2	Site3	Site4	Site5
k_{aA}^0 (activation)	L/(mol · s)	228.131	228.131	228.131	228.131	228.131
k_i^0 (initiation)	L/(mol · s)	4563	4563	4563	4563	4563
k_p^0 (propagation)	L/(mol · s)	2806.49	6890.73	8670.46	3650.72	798.595
k_{tH}^0 (transfer to hydrogen)	$L^{0.5}/(mol^{0.5} \cdot s)$	354.0	208.5	78.60	11.80	0.7780
k_{tM}^0 (transfer to monomer)	L/(mol · s)	0.00175	0.00175	0.00175	0.00175	0.00175
k_{tA}^0 (transfer to cocatalyst)	L/(mol · s)	0.00175	0.00175	0.00175	0.00175	0.00175
k_t^0 (transfer β-hydride)	/s	8×10^{-7}	8×10^{-7}	8×10^{-7}	8×10^{-7}	8×10^{-7}
k_d^0 (deactivation)	/s	4×10^{-5}	4×10^{-5}	4×10^{-5}	4×10^{-5}	4×10^{-5}

Table 3. Literature Data of Activation Energies in Homopolymerization

Reaction Types	Units	Site1	Site2	Site3	Site4	Site5
E^a_{aA} (activation)	kJ/mol	37.7	37.7	37.7	37.7	37.7
E^a_i (initiation)	kJ/mol	37.7	37.7	37.7	37.7	37.7
E^a_p (propagation)	kJ/mol	37.7	37.7	37.7	37.7	37.7
E^a_{tH} (transfer to hydrogen)	kJ/mol	58.6	58.6	58.6	58.6	58.6
E^a_{tM} (transfer to monomer)	kJ/mol	58.6	58.6	58.6	58.6	58.6
E^a_{tA} (transfer to cocatalyst)	kJ/mol	58.6	58.6	58.6	58.6	58.6
E^a_t (transfer β-hydride)	kJ/mol	58.6	58.6	58.6	58.6	58.6
E^a_d (deactivation)	kJ/mol	0	0	0	0	0

formation and development of MWD, while the transfer-to-hydrogen reaction mainly determines the position of the MWD at each site. Besides, we note that the HDPE reactor is operated isothermally at steady state and the temperature variation between different grades is small ($\leq 7^\circ C$). As a result, adding the activation energies in the Arrhenius equation to the parameter subset would not provide meaningful estimates from the given information. Therefore, only these two types of pre-exponential kinetic rate constants, k^0_p and k^0_{tH}, are selected as the estimated parameters and all the activation energies are left at their literature values. For the five-site catalyst system, this leads to 10 estimated kinetic parameters.

It should be noticed that this selection through the sensitivity coefficients only removes the least sensitive parameters from the estimation. The final subset of estimable parameters is obtained from the post-optimality analysis step below.

Post-Optimality Analysis. In the post-optimality analysis step, the preselected subset of estimable parameters could be further reduced after solving the parameter estimation problem. Confidence intervals of the current estimated parameters at the optimal point are computed for reliability evaluation. If the largest ratio of the confidence interval to the corresponding kinetic parameter exceeds a threshold, we update the subset by removing this parameter and reestimate with the new subset. The threshold β_2 is set here to 20%. This procedure continues until the largest confidence interval ratio is within the threshold.

Here, we obtain the confidence intervals of the kinetic parameters through the Hessian matrix at the optimal point. Generally, the confidence region can be expressed as[33]

$$\left\{\theta : (\theta-\theta^*)^T C(\theta^*)^{-1}(\theta-\theta^*) \leq N_\theta F^{1-\alpha}_{N_\theta,N-N_\theta}\right\} \qquad (28)$$

where θ is the estimated parameter vector, θ^* is the optimal estimated parameter vector, $C(\theta^*)$ is the covariance matrix at the optimal point, N_θ is the number of estimated parameters, N is the number of data points, and $F^{1-\alpha}_{N_\theta,N-N_\theta}$ is the upper α critical level of the $F_{N_\theta,N-N_\theta}$ distribution.

For nonlinear models where $w_{i,l}=1$, the covariance matrix $C(\theta^*)$ can be approximated as follows[34]

$$C(\theta^*)=\frac{2}{N-N_\theta}E(\theta^*)H(\theta^*)^{-1} \qquad (29)$$

where $E(\theta^*)$ and $H(\theta^*)$ are the objective function and the Hessian matrix at the optimal point, respectively. Then, the parameter confidence interval δ_i for the i th parameter is given by[34]

$$\delta_i=\pm t_{\alpha/2}(N-N_\theta)*\sqrt{C(\theta*)_{ii}} \quad i=1,...,N_\theta \qquad (30)$$

where $t_{\alpha/2}(N-N_\theta)$ is the two-tails Student's t distribution with α confidence level and $N-N_\theta$ degrees of freedom. The ratio of the confidence interval δ_i to the corresponding kinetic parameter is $r(\delta_i)$. Because this step is a postestimation analysis, the calculation of the parameter confidence intervals is based on the MWD data with white Gaussian noise from a simulation run below. In the simulation run, all the kinetic parameters are fixed to their literature values. Confidence level (95%) is used here. The results can be seen in Table 5. The estimated values and confidence intervals are scaled with the literature values of kinetic parameters in Table 2. For the initial 10 parameters, their scaled estimated values, confidence intervals, and interval ratios are shown in the second, third, and fourth columns of Table 5, respectively. Here, k^0_{tH} (Site 5) possesses the largest confidence interval ratio 106.4%, so it is removed from the subset and fixed to its literature value in the following estimation. The remaining nine parameters continue to be estimated and the results are shown in the fifth, sixth, and seventh columns of Table 5. k^0_{tH} (Site 4) possesses the largest confidence interval ratio 32.5%, so it is removed and fixed in the same way. Similarly, estimation is conducted for the left eight parameters. As shown in the eighth, ninth, and tenth columns of Table 5, now the largest ratio corresponding to k^0_p (Site 5) is only 14.3%, indicating that all the confidence intervals of these eight parameters meet the 20% ratio requirement and the parameter selection procedure stops. With this post-optimality analysis step, the reliability in the parameters can be greatly improved.

Multistep Methodology for Estimation

The parameter estimation problem derived from the HDPE slurry process is a large-scale NLP problem. The EO approach assembles all equations together, which results in the EO problem (26). According to the above analysis, two or more MWD profiles should be used as output variables in our cases to obtain reliable kinetic parameters. For the initial 10 estimated kinetic parameters, k^0_p (Site 1 to 5) and k^0_{tH}

Table 4. Data of Relative Sensitivity Coefficients of Different Kinetic Rate Constants from Eq. 27

	k_p	k_{tH}	k_{tM}	k_{tA}	k_t	k_d
τ_1	1.00×10^{0}	1.00×10^{0}	1.46×10^{-5}	3.09×10^{-8}	1.06×10^{-7}	5.20×10^{-6}
τ_2	1.00×10^{0}	1.00×10^{0}	2.48×10^{-5}	5.24×10^{-8}	1.80×10^{-7}	8.82×10^{-6}
τ_3	1.00×10^{0}	1.00×10^{0}	6.59×10^{-5}	1.39×10^{-7}	4.78×10^{-7}	2.34×10^{-5}
τ_4	1.00×10^{0}	1.00×10^{0}	4.39×10^{-4}	9.26×10^{-7}	3.18×10^{-6}	1.56×10^{-4}
τ_5	1.00×10^{0}	9.91×10^{-1}	6.60×10^{-3}	1.39×10^{-5}	4.78×10^{-5}	2.34×10^{-3}

Table 5. Data of Scaled Confidence Intervals of Kinetic Parameters at the Optimal Point (w/ Noise)

Parameters	Values	Intervals	Ratios	Values	Intervals	Ratios	Values	Intervals	Ratios
k_p^0 (Site 1)	0.9655	±0.0590	12.2%	0.9651	±0.0580	12.0%	0.9714	±0.0558	11.5%
k_p^0 (Site 2)	1.0005	±0.0406	8.1%	1.0000	±0.0386	7.7%	1.0112	±0.0280	5.5%
k_p^0 (Site 3)	0.9924	±0.0453	9.1%	0.9913	±0.0349	7.0%	1.0009	±0.0261	5.2%
k_p^0 (Site 4)	1.0572	±0.1121	21.2%	1.0582	±0.1089	20.6%	1.0125	±0.0199	3.9%
k_p^0 (Site 5)	1.0175	±0.3205	63.0%	1.0290	±0.0755	14.7%	1.0185	±0.0729	14.3%
k_{tH}^0 (Site 1)	0.9757	±0.0405	8.3%	0.9757	±0.0404	8.3%	0.9788	±0.0395	8.1%
k_{tH}^0 (Site 2)	1.0235	±0.0365	7.1%	1.0235	±0.0365	7.1%	1.0254	±0.0358	7.0%
k_{tH}^0 (Site 3)	1.0142	±0.0513	10.1%	1.0142	±0.0513	10.1%	1.0050	±0.0451	9.0%
k_{tH}^0 (Site 4)	1.0686	±0.2193	41.0%	1.0737	±0.1746	32.5%			
k_{tH}^0 (Site 5)	0.9806	±0.5219	106.4%						

(Site 1 to 5), structural statistics of problem (26) along with over 10,000 variables and equations are shown in Table 6, where four MWD profiles are used. The 10 degrees of freedom in the table correspond to the 10 estimated kinetic parameters. Intuitively, the kinetic parameters could be estimated by solving the minimization problem. However, problem (26) is hard to solve directly with any NLP algorithm. During the minimization process with IPOPT (Interior Point OPTimizer), a Newton-based solver, we observe that the KKT (Karush-Kuhn-Tucker) matrix of the problem is ill-conditioned, making the solution of the corresponding linear system of equations prone to large numerical errors. Consequently, direct solution leads to convergence failures, especially for poor problem initializations. Moreover, because the MWD calculation and the remaining process model are not strongly coupled to each other, we propose a multistep methodology that separates them into two parts by introducing a group of intermediate parameters. We will see that each part is less nonlinear, well-conditioned, and unique solutions can be computed with good efficiency and accuracy.

Step 1: Deconvolution

We first consider a set of modeling assumptions that lead to guiding constraints or regularization for this estimation step. Under the following reasonable assumptions:

- negligible concentrations of the active site and living polymer chain of unit length at each site in the reactor
- negligible transfer-to-monomer rate constant at each site compared to the propagation rate constant
- equal activation energies of propagation, concentrations of the potential active site, and the activation and deactivation rate constants at each site

we show in Appendix B that because $k_p^0(j)$ remains unchanged for each active site, the values of the polymer mole fractions at the same site j are the same under different sets of reactor operating conditions ((1), (2), (3), ..., (N_C)). As there is a slight deviation of the negligibility assumptions, we relax the equality of mf_j slightly. Consequently, we enforce the following regularization inequality, where we choose $\varepsilon = 0.01$ based on experience.

Table 6. Structural Statistics of the Original Estimation Problem

Definitions	Types	Values	Total
Variables	Nonlinear	8450	10557
	Linear	2107	
Equations	Nonlinear	2428	10547
	Linear	8119	
DOF	–	–	10

$$-\varepsilon \le (\mathrm{mf}_j(p) - \mathrm{mf}_j(q))/\mathrm{mf}_j(p) \le \varepsilon \quad p, q = 1, \ldots, N_C, p \ne q \tag{31}$$

In step 1, called the *deconvolution step*, we minimize the sum of the MWD deviations by adjusting the intermediate MWD parameters τ_j and mf_j.

$$\min_{\tau,\mathrm{mf}} \sum_{l=1}^{N_C}\sum_{m=1}^{N_P} \left[\overline{\mathrm{mwd}}(l)_{\mathrm{cal}}^m - \overline{\mathrm{mwd}}(l)_{\mathrm{tar}}^m\right]^2 \quad \text{s.t.} \quad \text{Equalities } (21), (22), (24) \quad \text{Inequality } (31) \tag{32}$$

The key constraints are the regularization inequality (31) along with the Flory's distribution equations, Eqs. 21, 22, and 24, which relate the MWD to τ_j and mf_j. However, the above assumptions and the inequality (31) are only used in this step to help regularize the optimization problem, and aid in estimation of reasonable MWD parameters. Numerical results below have shown that without (31), the values of τ_j and mf_j obtained in this step are severely biased when dealing with noise in MWDs. In the following steps, the regularization inequality (31) is no longer used and the kinetic parameters are estimated without these assumptions.

As the NLP (32) only contains the Flory's distribution equations, its scale and nonlinearity are reduced significantly compared with the original problem. Structural statistics of the deconvolution problem (four MWDs) are shown in Table 7. Problem (32) contains around 3000 variables and equations. The 36 degrees of freedom in the table correspond to the estimated MWD parameters. Here, we observe that the KKT matrix of the deconvolution problem is well-conditioned in all iterations during the solving procedure, and NLP solves very easily even with poor initial guesses.

Step 2: Process-solving

The second step, the *process-solving step*, minimizes the sum of the deviations between the calculated and the target values of τ_j and mf_j obtained from the optimal solution in the first step. This step obtains the estimated kinetic parameters that correspond to the optimal values of τ_j and mf_j by solving the following problem.

Table 7. Structural Statistics of the Deconvolution Problem

Definitions	Types	Values	Total
Variables	Nonlinear	1044	3044
	Linear	2000	
Equations	Nonlinear	2200	3008
	Linear	808	
DOF	–	–	36

Table 8. Structural Statistics of the Process-Solving Problem

Definitions	Types	Values	Total
Variables	Nonlinear	7442	7553
	Linear	111	
Equations	Nonlinear	228	7543
	Linear	7315	
DOF	–	–	10

$$\min_{k_p^0,k_{tH}^0} \sum_{l=1}^{N_C}\sum_{j=1}^{N_S}\left\{\left[(\tau(l)_j^{cal}-\tau(l)_j^{tar})/\tau(l)_j^{tar}\right]^2 + \left[(\mathrm{mf}\,(l)_j^{cal}-\mathrm{mf}\,(l)_j^{tar})/\mathrm{mf}\,(l)_j^{tar}\right]^2\right\} \quad (33)$$
$$\text{s.t.}\quad h_l\left(\tau(l)^{cal}, mf(l)^{cal}, k_p^0, k_{tH}^0\right)=0$$
$$l=1,\ldots,N_C$$

where $\tau(l)_j^{cal}$ and $\tau(l)_j^{tar}$ are the calculated and target values of τ at j th site under the l th set of reactor operating conditions, respectively. mf $(l)_j^{cal}$ and mf $(l)_j^{tar}$ are the calculated and target values of mf at j th site under the l th set of reactor operating conditions, respectively. The equality constraint h_l relates $\tau(l)^{cal}$ and mf $(l)^{cal}$ to the parameters k_p^0 and k_{tH}^0, which is the general model representation under the l th set of reactor operating conditions.

Because the NLP (33) contains the process model without the MWD calculation, its scale and nonlinearity are reduced compared with the original problem. Structural statistics of the process-solving problem along with around 7000 variables and equations are shown in Table 8. The 10 degrees of freedom in the table correspond to the initial 10 estimated kinetic parameters. Numerical results have shown that the KKT matrix of this part is well-conditioned for all iterations. Similarly, this problem can be solved very easily even with poor initial guesses.

Step 3: Re-estimation

The above two-step approach is much less sensitive to initial values and can find optimal solutions very easily. However, because the optimal solutions of the first two steps are obtained from separated parts of the original problem, the parameter estimates may not be good enough for optimal prediction with the complete process model. Numerical results have shown that the model description and prediction based on the estimated kinetic parameters of the first two steps are still biased when dealing with noise in MWDs. Hence, a third step, the *re-estimation step*, is used to obtain more accurate results. In this step, the original minimization problem (26) is solved directly with initial values from the results of the first two steps. Because the initial guesses are now very good, the ill-conditioned minimization problem converges quickly for the original problem (26). The resulting parameter estimates are more accurate due to the overall consideration of the complete EO optimization model.

The flowchart of the multistep strategy is outlined in Figure 3. The basic idea is to separate a highly nonlinear, ill-conditioned problem into two well-conditioned subproblems by introducing the intermediate MWD parameters. As seen from the numerical results below, this strategy achieves fast convergence in finding optimal solutions.

Results and Discussion

In this project, AMPL (A Mathematical Programming Language), an EO optimization modeling system, was used to construct the complete problem formulation. The problems were numerically solved using IPOPT 3.10.1 on Dell T3500 running 64-bit Windows 7 with a 2.40 GHz Intel Xeon processor and 14 GB RAM. In IPOPT, uniqueness of the optimal solution has been confirmed through nonsingularity of the KKT matrix at the solution. If the KKT matrix is singular (more specifically, if sufficient second-order conditions are not satisfied and the reduced Hessian is not positive definite), then this matrix is augmented with a regularization parameter at the solution. In all the cases below, no regularization was ever required at the optimal point, indicating that sufficient second-order conditions are satisfied and the solution is at least locally unique and isolated. This is an important property inherent in IPOPT, as described in Zavala et al.[35]

Estimation using simulation results

Several estimation cases based on the numerical results of a simulation run are first presented. In the simulation run, all the kinetic parameters are fixed to the literature values in Tables 2 and 3. For the serial flow sheet with two CSTRs, hypothetical HDPE grades G and O, including two intermediate grades out of the first reactor (G(R1) and O(R1)) and two product grades out of the second reactor (G(R2) and O(R2)), are considered. The intermediate polymer produced in the first reactor can be sampled so that its MWD is

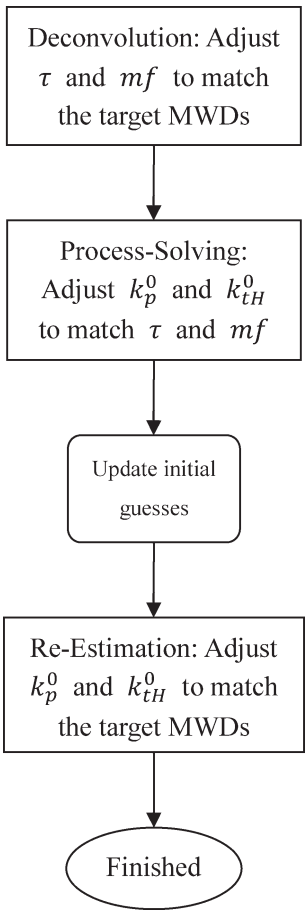

Figure 3. Flowchart of the multistep methodology.

Table 9. Data of the Feed Streams and Reactors for Simulation

Subsystems	Properties	G(R1)	G(R2)	O(R1)	O(R2)
Catalyst	T (K)	293.15	–	293.15	–
	P (kPa)	1301.0	–	1301.0	–
	FR (kmol/h)	0.49	–	0.30	–
	x_{TiCl_4}	0.00101	–	0.00131	–
	$x_{C_6H_{14}}$	0.99899	–	0.99869	–
Cocatalyst	T (K)	293.15	–	293.15	–
	P (kPa)	1301.0	–	1301.0	–
	FR (kmol/h)	0.84	–	0.85	–
	x_A	0.003	–	0.003	–
	$x_{C_6H_{14}}$	0.997	–	0.997	–
Ethylene	T (K)	318.15	318.15	318.15	318.15
	P (kPa)	1301.0	1301.0	1301.0	1301.0
	FR (kmol/h)	125.89	95.17	123.35	99.78
Hydrogen	T (K)	273.15	273.15	273.15	273.15
	P (kPa)	100.31	100.31	100.31	100.31
	FR (kmol/h)	4.05	0.09	3.34	0.15
Hexane	T (K)	313.15	313.15	313.15	313.15
	P (kPa)	1301.0	1301.0	1301.0	1301.0
	FR (kmol/h)	38.43	14.66	38.17	12.88
Re-Hexane	T (K)	343.15	343.15	343.15	343.15
	P (kPa)	1301.0	1301.0	1301.0	1301.0
	FR (kmol/h)	58.19	53.82	57.34	56.49
Reactors	T (K)	358.15	351.15	358.03	353.15
	P (kPa)	803.51	330.32	721.43	399.22
	V (m^3)	30.60	30.15	30.47	29.16

measurable. For these grades, there are four corresponding sets of steady-state operating conditions. The information on the feed streams and reactors for the flow sheet is given in Table 9, where T represents temperature, P represents pressure, FR represents flow rate, V represents liquid volume, and x represents the mole fraction of a component. As shown in Table 9, the major differences between these sets of operating conditions are the pressure and the flow rates of introduced hydrogen of reactors. The resulting values of mf under different operating conditions are almost the same, as indicated in the regularization inequality (31). The details can be seen in the second columns of Tables 10 and 11. All four resulting MWDs (with 5% white Gaussian noise or not) from the first and second reactors are used as the target MWDs, as seen in Figure 4, where "w/ Noise" means MWDs with Gaussian noise, and "w/o Noise" means MWDs without noise. The selected pre-exponential constants are supposed unknown and estimated. It is expected the optimal values of the estimated parameters are almost the same as the "true values" in the simulation.

MWDs Without Noise. We first tried to solve NLP (26) using four noise-free MWD profiles (w/o Noise). However, the direct approach failed to converge; instead, the multistep methodology was used. In the *deconvolution step*, IPOPT required 104 iterations and 1.5 CPU s to solve problem (32). The value of MWD deviations is 4.20×10^{-16}, equivalent to zero to numerical precision, and the decision variables, τ and mf , converged to a unique optimal point, as seen in the fourth column of Table 10. The values are exactly the same as the true values in the simulation run. Moreover, when constraint (31) is removed, the same result is obtained, as seen in the third column of Table 10. In the *process-solving step*, the target values in the objective function are exactly the same as the optimal values obtained from the first step with constraint (31). For the final eight estimated kinetic parameters, k_p^0 (Site 1 to 5) and k_{tH}^0 (Site 1 to 3), IPOPT required 18 iterations and 4.1 CPU s to solve problem (33). The value of MWD deviations is 3.92×10^{-13}, equivalent to zero to numerical precision, and the eight pre-exponential kinetic rate constants converged to a unique optimal point. These values can be seen in the third column of Table 12, which are exactly the same as the true values of kinetic parameters in the simulation run. Moreover, the corresponding values of τ and mf are exactly the same as the true values in the simulation run, as seen in the fifth column of Table 10. In the *re-estimation step*, structural statistics of the re-estimation problem are the same as that of problem (26). Because the initial guesses are now very good, the original problem can converge very quickly. IPOPT required 15 iterations and 7.8 CPU s to solve it. The value of MWD deviations is 8.19×10^{-19}, equivalent to zero to numerical precision, and the eight pre-exponential kinetic rate constants, converged to a unique optimal point. These values can be seen in the fourth column of Table 12, which are exactly the same as the true values of kinetic parameters in the simulation run. Also, the corresponding values of τ and mf are exactly the same as the true values in the simulation run, as seen in the sixth column of Table 10. Comparisons between the optimized and target noise-free MWDs are illustrated in Figure 5. The thick lines represent the target noise-free MWDs in the simulation run, the dashed lines are the optimized MWDs in the first step, the thin lines are the optimized MWDs in the second step, and the dash-dotted lines are the optimized MWDs in the third step. They coincide with each other perfectly.

MWDs with Noise. The cases with noise are designed to observe the practical performance of this methodology. We first tried to solve the original estimation problem (26) using four MWD profiles with 5% white Gaussian noise (w/ Noise). Because the direct approach failed to converge, the multistep methodology was used. In the *deconvolution step*, IPOPT required 155 iterations and 2.3 CPU s to solve problem (32). The value of MWD deviations from the noise-free target profiles is 3.90×10^{-3}, which is much larger than that in the noise-free case. The decision variables, τ and mf ,

Table 10. Data of MWD Parameters in the Case Without Noise

Parameters	Simulation	Step 1 Without (31)	Step 1 With (31)	Step 2	Step 3
τ_1(G(R1))	0.042633	0.042633	0.042633	0.042633	0.042633
τ_2(G(R1))	0.010227	0.010227	0.010227	0.010227	0.010227
τ_3(G(R1))	0.003064	0.003064	0.003064	0.003064	0.003064
τ_4(G(R1))	0.001093	0.001093	0.001093	0.001093	0.001093
τ_5(G(R1))	0.000332	0.000332	0.000332	0.000332	0.000332
mf_1(G(R1))	0.125040	0.125040	0.125040	0.125040	0.125040
mf_2(G(R1))	0.300623	0.300623	0.300623	0.300623	0.300623
mf_3(G(R1))	0.379179	0.379179	0.379179	0.379179	0.379179
mf_4(G(R1))	0.160128	0.160128	0.160128	0.160128	0.160128
mf_5(G(R1))	0.035030	0.035030	0.035030	0.035030	0.035030
τ_1(G(R2))	0.000446	0.000446	0.000446	0.000446	0.000446
τ_2(G(R2))	0.000107	0.000107	0.000107	0.000107	0.000107
τ_3(G(R2))	0.000032	0.000032	0.000032	0.000032	0.000032
τ_4(G(R2))	0.000012	0.000012	0.000012	0.000012	0.000012
τ_5(G(R2))	0.000006	0.000006	0.000006	0.000006	0.000006
mf_1(G(R2))	0.124220	0.124220	0.124220	0.124220	0.124220
mf_2(G(R2))	0.301177	0.301177	0.301177	0.301177	0.301177
mf_3(G(R2))	0.379509	0.379509	0.379509	0.379509	0.379509
mf_4(G(R2))	0.160077	0.160077	0.160077	0.160077	0.160077
mf_5(G(R2))	0.035018	0.035018	0.035018	0.035018	0.035018
τ_1(O(R1))	0.028116	0.028116	0.028116	0.028116	0.028116
τ_2(O(R1))	0.006745	0.006745	0.006745	0.006745	0.006745
τ_3(O(R1))	0.002021	0.002021	0.002021	0.002021	0.002021
τ_4(O(R1))	0.000721	0.000721	0.000721	0.000721	0.000721
τ_5(O(R1))	0.000220	0.000220	0.000220	0.000220	0.000220
mf_1(O(R1))	0.124356	0.124356	0.124356	0.124356	0.124356
mf_2(O(R1))	0.301086	0.301086	0.301086	0.301086	0.301086
mf_3(O(R1))	0.379455	0.379455	0.379455	0.379455	0.379455
mf_4(O(R1))	0.160084	0.160084	0.160084	0.160084	0.160084
mf_5(O(R1))	0.035020	0.035020	0.035020	0.035020	0.035020
τ_1(O(R2))	0.000420	0.000420	0.000420	0.000420	0.000420
τ_2(O(R2))	0.000101	0.000101	0.000101	0.000101	0.000101
τ_3(O(R2))	0.000030	0.000030	0.000030	0.000030	0.000030
τ_4(O(R2))	0.000011	0.000011	0.000011	0.000011	0.000011
τ_5(O(R2))	0.000006	0.000006	0.000006	0.000006	0.000006
mf_1(O(R2))	0.123793	0.123793	0.123793	0.123793	0.123793
mf_2(O(R2))	0.301465	0.301465	0.301465	0.301465	0.301465
mf_3(O(R2))	0.379681	0.379681	0.379681	0.379681	0.379681
mf_4(O(R2))	0.160049	0.160049	0.160049	0.160049	0.160049
mf_5 (O(R2))	0.035012	0.035012	0.035012	0.035012	0.035012

also converged to a unique optimal point, as seen in the fourth column of Table 11. However, the optimal values are not exactly the same as the ones in the simulation run. Moreover, if constraint (31) is removed, the resulting parameters in this step are not determined uniquely, as seen in the third column of Table 11. For the final eight estimated kinetic parameters, k_p^0 (Site 1 to 5) and k_{tH}^0 (Site 1 to 3), IPOPT required 19 iterations and 3.8 CPU s to solve problem (33) in the *process-solving step*. The value of MWD deviations from the noise-free target profiles is 3.01×10^{-3}, and the eight pre-exponential kinetic rate constants converged to a unique optimal point, as seen in the fifth column of Table 12. However, because of the influence of the white Gaussian noise, the optimal values are not exactly the same as the ones in the simulation run. The corresponding values of τ and mf can be seen in the fifth column of Table 11. Finally, in the *re-estimation step*, IPOPT required 24 iterations and 7.0 CPU s to solve problem (26). The value of MWD deviations from the noise-free target profiles is 1.12×10^{-3}, and the eight pre-exponential kinetic rate constants converged to a unique optimal point, as seen in the sixth column of Table 12. The corresponding values of τ and mf can be seen in the sixth column of Table 11. Comparisons between the optimized and target noise-free MWDs are illustrated in Figure 6. In the first step, one does not get a perfect agreement between the thick and dashed lines, especially in the summit regions. In the second step, the thin lines still do not fit the target MWD perfectly. This justifies the additional *re-estimation step* which improves the fitting and obtains more accurate results. In the third step, the dash-dotted lines achieve excellent agreement with the solid lines. The improvement of the practical performance can also be observed from the values of MWD deviations in the second and third step (3.01×10^{-3} and 1.12×10^{-3}). From these results, we observe the multistep methodology achieves fast convergence in finding optimal parameter estimates.

Lagrange Hessian analysis

Analysis of the Hessian matrix of the Lagrange function highlights important information about the modeling problem characteristics. Specifically, response surfaces of the Lagrange function in the neighborhood of a local minimum are determined by the Hessian eigensystem that describes the directions of principal curvature and the amount of curvature in each direction. Moreover, the ratio between the highest and lowest eigenvalues defines the condition number. When the condition number is equal to 1, contours of the Lagrange function are circular; as the condition number increases, the elliptical contours become more elongated. A large condition number denotes an ill-conditioned problem, where the

Table 11. Data of MWD Parameters in the Case with Noise

Parameters	Simulation	Step 1 without (31)	Step 1 with (31)	Step 2	Step 3
τ_1(G(R1))	0.042633	0.045721	0.044024	0.043504	0.043239
τ_2(G(R1))	0.010227	0.011350	0.010844	0.010322	0.010503
τ_3(G(R1))	0.003064	0.003358	0.003146	0.003063	0.003146
τ_4(G(R1))	0.001093	0.001225	0.001121	0.001092	0.001113
τ_5(G(R1))	0.000332	0.000348	0.000318	0.000322	0.000324
mf_1(G(R1))	0.125040	0.112878	0.119697	0.120996	0.120480
mf_2(G(R1))	0.300623	0.292029	0.300153	0.299691	0.299749
mf_3(G(R1))	0.379179	0.364268	0.376304	0.376228	0.374845
mf_4(G(R1))	0.160128	0.189179	0.167416	0.166902	0.168979
mf_5(G(R1))	0.035030	0.041647	0.036430	0.036182	0.035947
τ_1(G(R2))	0.000446	0.002730	0.000526	0.000482	0.000459
τ_2(G(R2))	0.000107	0.000531	0.000121	0.000114	0.000112
τ_3(G(R2))	0.000032	0.000124	0.000034	0.000034	0.000034
τ_4(G(R2))	0.000012	0.000033	0.000013	0.000013	0.000012
τ_5(G(R2))	0.000006	0.000010	0.000006	0.000006	0.000006
mf_1(G(R2))	0.124220	0.007263	0.118496	0.120157	0.119637
mf_2(G(R2))	0.301177	0.104513	0.297150	0.300265	0.300320
mf_3(G(R2))	0.379509	0.302716	0.380069	0.376558	0.375178
mf_4(G(R2))	0.160077	0.413965	0.167479	0.166851	0.168929
mf_5(G(R2))	0.035018	0.171543	0.036807	0.036170	0.035935
τ_1(O(R1))	0.028116	0.026731	0.027560	0.028726	0.028524
τ_2(O(R1))	0.006745	0.006276	0.006633	0.006816	0.006929
τ_3(O(R1))	0.002021	0.001896	0.002057	0.002023	0.002075
τ_4(O(R1))	0.000721	0.000633	0.000718	0.000721	0.000734
τ_5(O(R1))	0.000220	0.000174	0.000209	0.000214	0.000215
mf_1(O(R1))	0.124356	0.127241	0.120898	0.120300	0.119778
mf_2(O(R1))	0.301086	0.318978	0.302951	0.300167	0.300225
mf_3(O(R1))	0.379455	0.379172	0.373605	0.376503	0.375124
mf_4(O(R1))	0.160084	0.144205	0.165739	0.166858	0.168936
mf_5(O(R1))	0.035020	0.030405	0.036807	0.036172	0.035937
τ_1(O(R2))	0.000420	0.007141	0.000435	0.000453	0.000432
τ_2(O(R2))	0.000101	0.000443	0.000101	0.000108	0.000105
τ_3(O(R2))	0.000030	0.000123	0.000031	0.000032	0.000032
τ_4(O(R2))	0.000011	0.000036	0.000011	0.000012	0.000012
τ_5(O(R2))	0.000006	0.000011	0.000006	0.000006	0.000006
mf_1(O(R2))	0.123793	0.003198	0.122111	0.119723	0.119199
mf_2(O(R2))	0.301465	0.120546	0.299920	0.300561	0.300617
mf_3(O(R2))	0.379681	0.233298	0.375063	0.376729	0.375352
mf_4(O(R2))	0.160049	0.411358	0.166481	0.166823	0.168903
mf_5(O(R2))	0.035012	0.231600	0.036426	0.036163	0.035929

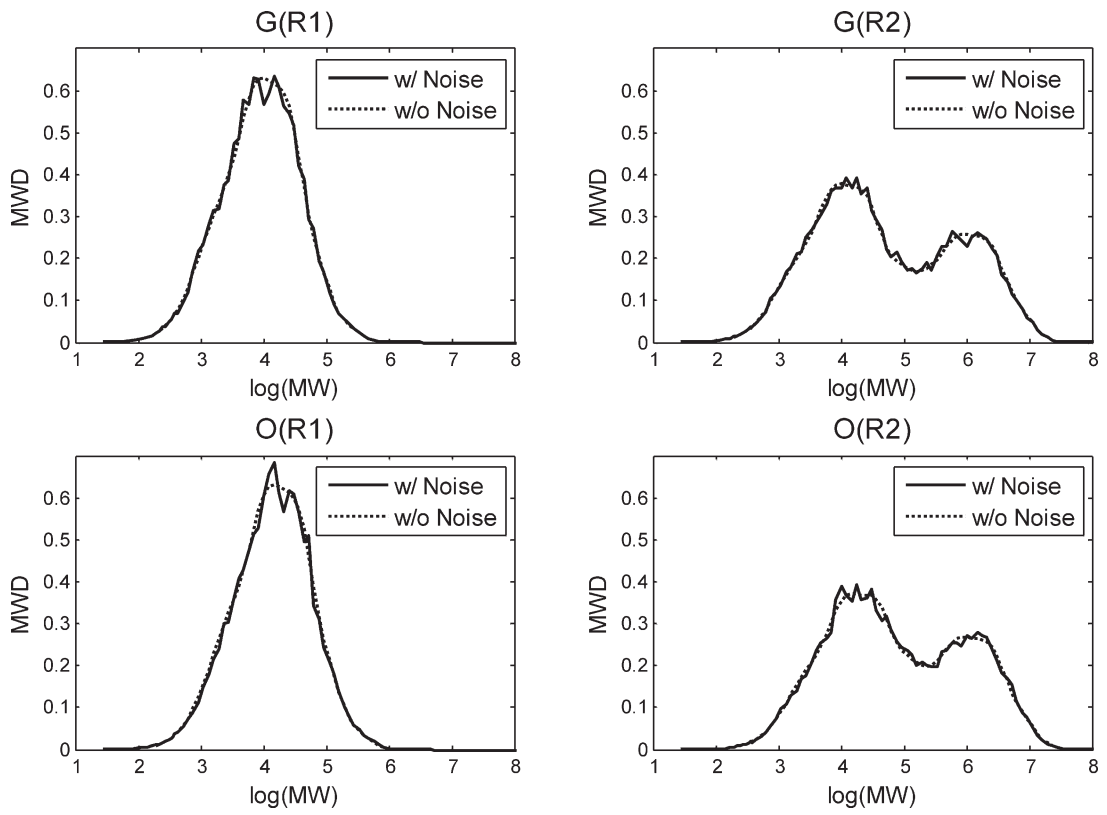

Figure 4. Simulation results: target MWDs without and with 5% Gaussian noise (G(R1): Grade G, Reactor 1; G(R2): Grade G, Reactor 2; O(R1): Grade O, Reactor 1; O(R2): Grade O, Reactor 2).

Table 12. Data of Estimated Kinetic Parameters

Parameters	Simulation	Step 2 (w/o Noise)	Step 3 (w/o Noise)	Step 2 (w/ Noise)	Step 3 (w/ Noise)	Industrial Case
k_p^0 (Site 1)	2806.49	2806.49	2806.49	2753.12	2726.25	2509.78
k_p^0 (Site 2)	6890.73	6890.73	6890.73	6983.76	6967.62	6334.02
k_p^0 (Site 3)	8670.46	8670.46	8670.46	8752.64	8678.41	8825.47
k_p^0 (Site 4)	3650.72	3650.72	3650.72	3796.38	3696.37	3285.53
k_p^0 (Site 5)	798.595	798.597	798.595	837.008	813.397	702.435
k_{tH}^0 (Site 1)	354.0	354.0	354.0	347.3	346.5	456.1
k_{tH}^0 (Site 2)	208.5	208.5	208.5	209.0	213.8	266.5
k_{tH}^0 (Site 3)	78.60	78.60	78.60	77.72	78.99	103.7

Lagrange function can change radically depending on the direction of variable perturbations.

The above estimation cases (w/ Noise) were used to analyze the conditioning of our problems. Since the optimal solution of NLP (26) had been obtained in the *re-estimation step*, we calculated its Lagrange Hessian with respect to the kinetic parameters at the solution. For the initial 10 estimated parameters, the corresponding 10 Hessian eigenvalues can be seen in the third column of Table 13. The condition number is 10052.8 with several near-zero eigenvalues. Note that the objective function may vary very slowly along an eigenvector associated with a near-zero eigenvalue and changes in the objective function may be lost amongst the rounding error. The ill-conditioning also causes degradation in performance of NLP methods (e.g., IPOPT, CONOPT) that need to solve the KKT system. Corresponding to the two kinetic parameters, k_p^0 (Site 1) and k_{tH}^0 (Site 5), Figure 7 presents the contours of the objective function near the optimal point. The response surface is a long, narrow valley, and gradients change quickly down the valley walls, but very slowly along the valley floor. When initial guesses are poor, NLP methods experience convergence failures due to the ill-conditioned characteristics. However, when the initial point is close to the optimal point, we can obtain the solution reasonably efficiently, as seen in the *re-estimation step*.

As a comparison, we calculated the Hessian with respect to all 10 kinetic parameters at the solution in the *process-solving step* (33). The 10 Hessian eigenvalues can be seen in the second column of Table 13. The condition number is 61.8, which is much smaller than that in the original problem. Also, there are no near-zero eigenvalues. Corresponding to the same two kinetic parameters, the contours of the objective function near the optimal point are shown in Figure 8, where the response surface is almost circular. We also calculated the Hessian with respect to all 36 independent MWD parameters at the solution in the *deconvolution step* (32). The 36 Hessian eigenvalues can be seen in the first column of Table 13. The highest and lowest values are 1.6×10^9 and 0.34, respectively. However, while the highest eigenvalue has a large magnitude, there are no near-zero

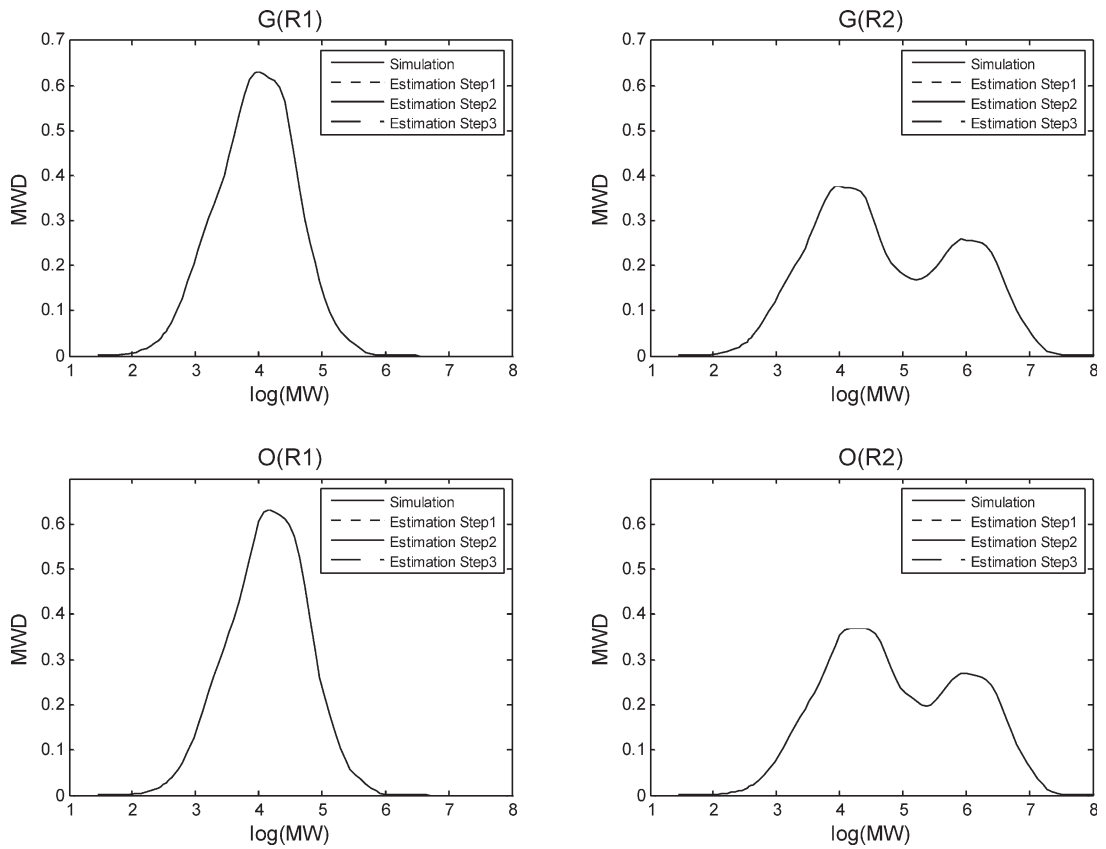

Figure 5. Estimation results: MWD comparisons between different steps in the case without noise (G(R1), G(R2), O(R1), O(R2)).

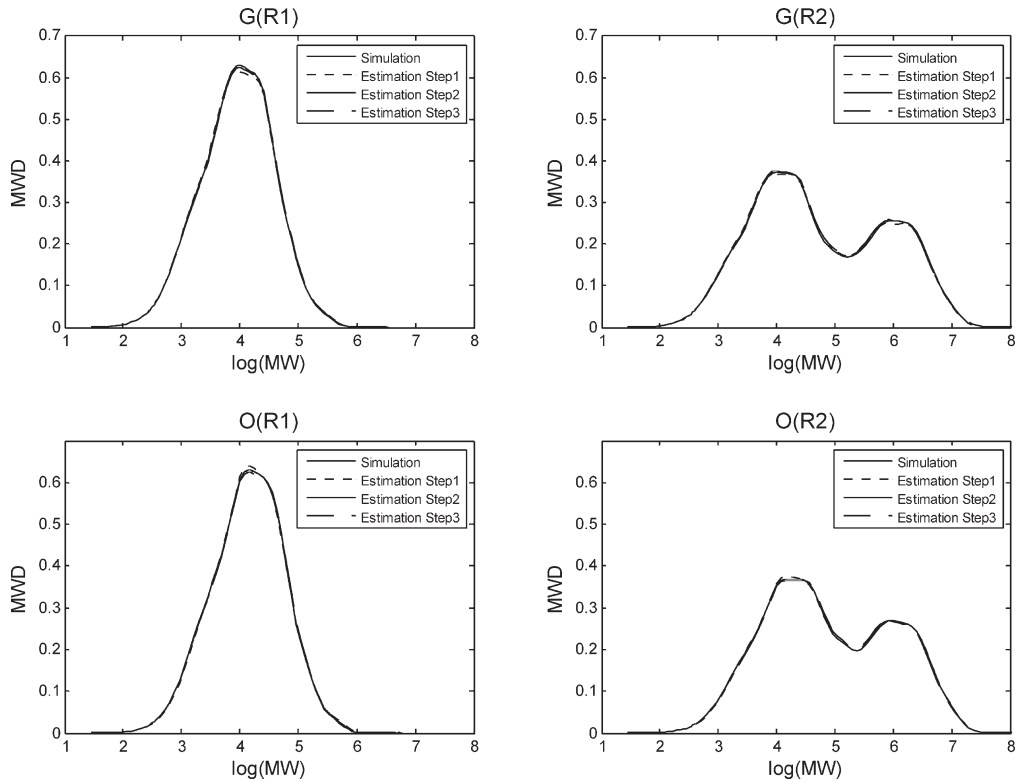

Figure 6. Estimation results: MWD comparisons between different steps in the case with noise (G(R1), G(R2), O(R1), O(R2)).

Table 13. Data of Lagrange Hessian Eigenvalues at the Optimal Point (w/ Noise)

Step 1	Step 2	Step 3
3.44504×10^{-1}	2.29569×10^{0}	2.17155×10^{-3}
4.53770×10^{-1}	2.65902×10^{0}	2.11490×10^{-2}
4.70206×10^{-1}	2.96508×10^{0}	1.46572×10^{-1}
5.75561×10^{-1}	3.02900×10^{0}	2.27711×10^{-1}
6.75807×10^{-1}	3.79209×10^{0}	3.64848×10^{-1}
1.08013×10^{0}	1.59938×10^{1}	7.21746×10^{-1}
1.22038×10^{0}	1.84925×10^{1}	3.41412×10^{0}
1.22977×10^{0}	2.04312×10^{1}	6.13020×10^{0}
2.26192×10^{0}	2.07727×10^{1}	1.00958×10^{1}
2.37689×10^{0}	1.42275×10^{2}	2.46142×10^{1}
3.15262×10^{0}		
3.92628×10^{0}		
4.45243×10^{0}		
6.44491×10^{0}		
7.84931×10^{0}		
1.84355×10^{1}		
2.42768×10^{1}		
8.45116×10^{1}		
1.63929×10^{2}		
4.88597×10^{2}		
1.49436×10^{4}		
5.97176×10^{4}		
1.00205×10^{5}		
2.04604×10^{5}		
2.27817×10^{5}		
5.28010×10^{5}		
5.45764×10^{5}		
7.68917×10^{5}		
1.21511×10^{6}		
1.49254×10^{6}		
1.17723×10^{7}		
1.80054×10^{7}		
4.52605×10^{8}		
4.96160×10^{8}		
1.04212×10^{9}		
1.62928×10^{9}		

eigenvalues. Corresponding to the 16 very high eigenvalues (from 1.5×10^{4} to 1.6×10^{9}), steep gradients prevent any movement along the corresponding eigendirections, and essentially remove these dimensions from the problem. As the remaining eigenvalues are bounded away from zero, the problem is well-conditioned. The characteristics of the first two steps make it much easier for NLP algorithms to find

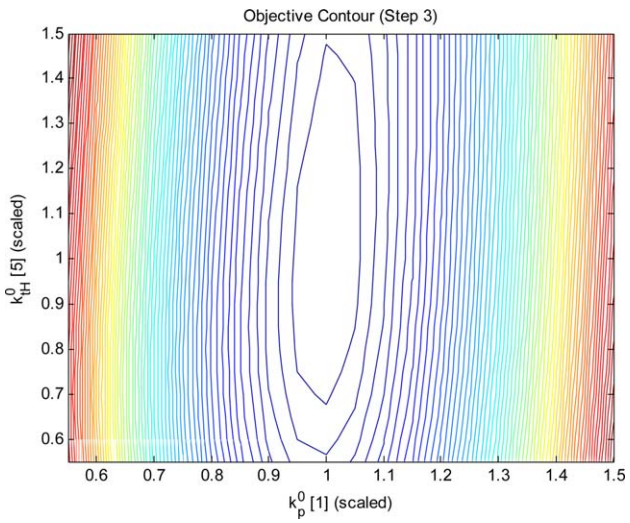

Figure 7. Objective function contours on the coordinate plane determined by scaled kinetic parameters k^0_p (Site 1) and k^0_{tH} (Site 5) near the optimal point (Step 3).

[Color figure can be viewed in the online issue, which is available at wileyonlinelibrary.com.]

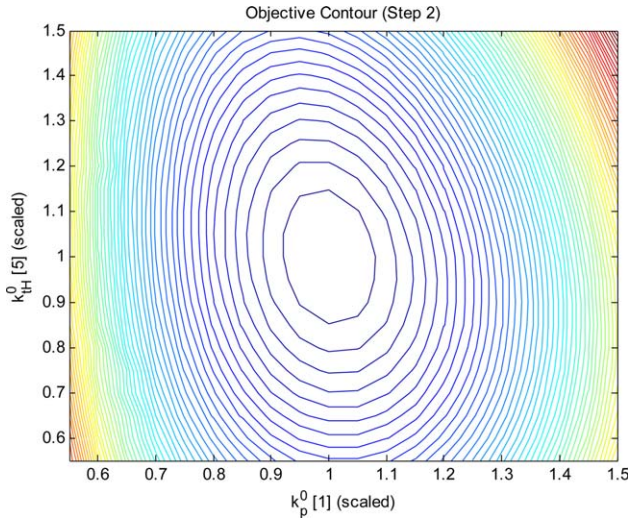

Figure 8. Objective function contours on the coordinate plane determined by scaled kinetic parameters k_p^0 (Site 1) and k_{tH}^0 (Site 5) near the optimal point (Step 2).

[Color figure can be viewed in the online issue, which is available at wileyonlinelibrary.com.]

the optimal point. This analysis indicates how this methodology separates an ill-conditioned problem into two well-conditioned subproblems, thus improving the efficiency and accuracy of problem solving.

Industrial case study

Finally, we considered the kinetic parameter estimation problem at an industrial scale. HDPE grades, PG and PO, were produced in the industrial process in Figure 1. Using the corresponding real plant data, the same eight pre-exponential kinetic rate constants were selected and estimated while the others were fixed as their literature values. The operating conditions in the EO model were set to those measured in the real process. The objective was to minimize the deviation of the calculated MWDs from their offline gel permeation chromatography (GPC) measurements. As seen in Figure 9, the four "GPC" curves of PG(R1), PO(R1), PG(R2), and PO(R2), which were the measurements of the first and second reactors, were used as the target MWD profiles. The eight pre-exponential kinetic rate constants converged to a unique optimal point, as seen in the seventh column of Table 12. The comparisons between the target and optimized MWDs are illustrated in Figure 9. Considering the fact that the relative error of the GPC measurements could be approximately 10%, we can see fairly good agreement is between the MWDs as the maximum relative error between the curves is less than 7% for both grades. The results show that the optimized kinetic parameters can be fitted successfully to the actual industrial process.

Conclusions

A steady-state EO model has been developed for an HDPE slurry process. Based on this model, an estimability analysis is conducted to determine relatable output variables and estimable kinetic parameters. The comparison between scalar properties and MWD shows we could estimate kinetic parameters using the information of MWDs with limited data to obtain more accurate results. Also, a systematic approach using relative sensitivity coefficients and confidence intervals is addressed to obtain a subset of estimable kinetic parameters. Then, the MWD fitting problem is formulated to determine the optimal kinetic parameters. However, solving the ill-conditioned original problem directly tends to cause convergence failures. Instead, a new multistep methodology, including the *deconvolution*, *process-solving*, and *re-estimation steps*, is introduced to solve the problems more efficiently. In addition, analysis of the Hessian matrix

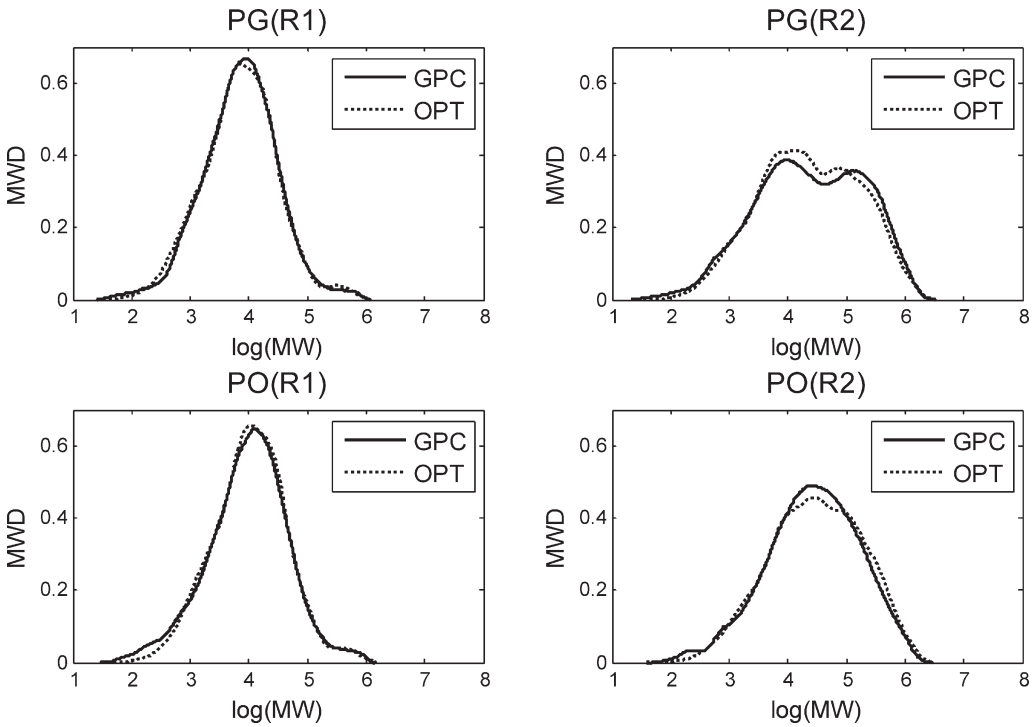

Figure 9. Estimation results: MWD comparisons in the industrial case.

of the Lagrange function indicates that the multistep methodology separates an ill-conditioned problem into well-conditioned subproblems. Three large-scale case studies, including an industrial case, have also been presented. This methodology shows significant advantages in convergence behavior and computational effort, and the numerical results demonstrate the effectiveness of the optimization performance to obtain accurate kinetic parameter estimates. Moreover, our multistep methodology, which introduces a group of MWD parameters (τ and mf), offers a new direction for solution of parameter estimation problems. We believe that this approach can be generalized to other systems where the model structure can be exploited by introducing a similar group of intermediate parameters as the new input (e.g. lumped parameters) or output variables for estimation. Thus, other models could be decomposed to improve the efficiency and accuracy of problem solving.

Acknowledgments

We gratefully acknowledge the financial support of 973 Program of China (No. 2012CB720503), National Natural Science Foundation of China (Nos. 61374205 & 61374167), and 863 Program of China (No. 2012AA040305).

Notation

A = cocatalyst
β_1 = threshold for pre-selection
β_2 = threshold for post-optimality analysis
$\mathrm{C_6H_{14}}$ = n-hexane
$C_\mathrm{d}(j)$ = deactivated site j of catalyst
$C_\mathrm{P}(j)$ = potential active site j of catalyst
C_L^U = total concentration of liquid flow out of unit U, mol/L
$C_\mathrm{Lin}^\mathrm{U}$ = total concentration of liquid flow into unit U, mol/L
C_V^U = total concentration of vapor flow out of unit U, mol/L
$C_\mathrm{Vin}^\mathrm{U}$ = total concentration of vapor flow into unit U, mol/L
cld_j = weight chain length distribution at site j
CO = components: M, $\mathrm{H_2}$, and $\mathrm{C_6H_{14}}$
$C(\theta)$ = covariance matrix at point θ
$D_n(j)$ = dead polymer of chain length n at site j
δ_i = parameter confidence interval for the ith parameter
E^a = activation energy, kJ/mol
E_f = compressor isentropic efficiency
$E(\theta)$ = objective function at point θ
ε = mole fraction inequality tolerance
F_L^U = liquid flow rate out of unit U, L/s
$F_\mathrm{Lin}^\mathrm{U}$ = liquid flow rate fed into unit U, L/s
F_V^U = vapor flow rate out of unit U, L/s
$F_\mathrm{Vin}^\mathrm{U}$ = vapor flow rate fed into unit U, L/s
FR = flow rate of a component, kmol/h
$F_{N_\theta,N-N_\theta}^{1-\alpha}$ = upper α critical level of the $F_{N_\theta,N-N_\theta}$ distribution.
$\varphi_\mathrm{L,CO}^\mathrm{U}$ = liquid-phase fugacity coefficient of component CO in unit U, kPa
$\varphi_\mathrm{V,CO}^\mathrm{U}$ = vapor-phase fugacity coefficient of component CO in unit U, kPa
$G_{i,l}$ = equations relating $y(i,l)_\mathrm{cal}$ to z under the lth set of operating conditions
g_l = equations relating $\mathrm{mwd}\,(l)_\mathrm{cal}$ to k_p^0, k_tH^0 under the lth set of operating conditions
h_l = equations relating $\tau(l)^\mathrm{cal}$, $\mathrm{mf}\,(l)^\mathrm{cal}$ to k_p^0, k_tH^0 under the lth set of operating conditions
$\mathrm{H_2}$ = hydrogen
H_L^U = enthalpy of liquid flow out of unit U, kJ/mol
$H_\mathrm{Lin}^\mathrm{U}$ = enthalpy of liquid flow into unit U, kJ/mol
H_V^U = enthalpy of vapor flow out of unit U, kJ/mol
$H_\mathrm{Vin}^\mathrm{U}$ = enthalpy of vapor flow into unit U, kJ/mol
$H_\mathrm{S}^\mathrm{Comp}$ = isentropic enthalpy of vapor flow out of the compressor, kJ/mol
$H(\theta)$ = Hessian matrix at point θ
i = index of output variables
j = index of catalyst active sites
k = general kinetic rate constant, L/(mol·s), $\mathrm{L}^{0.5}/(\mathrm{mol}^{0.5}\cdot\mathrm{s})$, s^{-1}
k^0 = general pre-exponential kinetic rate constant, L/(mol·s), $\mathrm{L}^{0.5}/(\mathrm{mol}^{0.5}\cdot\mathrm{s})$, s^{-1}
$k(j)$ = general kinetic rate constant at site j, L/(mol·s), $\mathrm{L}^{0.5}/(\mathrm{mol}^{0.5}\cdot\mathrm{s})$, s^{-1}
$k_\mathrm{aA}(j)$ = kinetic rate constant of activation at site j, L/(mol·s)
$k_\mathrm{d}(j)$ = kinetic rate constant of deactivation at site j, s^{-1}
$k_\mathrm{i}(j)$ = kinetic rate constant of initiation at site j, L/(mol·s)
$k_\mathrm{p}(j)$ = kinetic rate constant of propagation at site j, L/(mol·s)
$k_\mathrm{t}(j)$ = kinetic rate constant of transfer β-hydride at site j, s^{-1}
$k_\mathrm{tA}(j)$ = kinetic rate constant of transfer to cocatalyst at site j, L/(mol·s)
$k_\mathrm{tH}(j)$ = kinetic rate constant of transfer to hydrogen at site j, $\mathrm{L}^{0.5}/(\mathrm{mol}^{0.5}\cdot\mathrm{s})$
$k_\mathrm{tM}(j)$ = kinetic rate constant of transfer to monomer at site j, L/(mol·s)
$K_\mathrm{TD}(j)$ = pseudokinetic rate constant of transfer and deactivation at site j, s^{-1}
l = index of sets of operating conditions
M = monomer
m = index of sampling points on MWD curve
m_1 = polymer mass of the first reactor, kg/s
m_2 = polymer mass of the second reactor, kg/s
mf_j = mole fraction of the polymer produced at site j
$\mathrm{mf}(l)_j^\mathrm{cal}$ = calculated mf at site j under the lth set of operating conditions
$\mathrm{mf}\,(l)_j^\mathrm{tar}$ = target mf at site j under the lth set of operating conditions
mw = molecular weight of ethylene, 28.05 g/mol
MWD = molecular weight distribution of the final product
mwd_j = molecular weight distribution at site j on the logarithmic scale of molecular weight
$\overline{\mathrm{mwd}}$ = molecular weight distribution of one reactor
$\overline{\mathrm{mwd1}}$ = molecular weight distribution of the first reactor
$\overline{\mathrm{mwd2}}$ = molecular weight distribution of the second reactor
$\overline{\mathrm{mwd}}\,(l)_\mathrm{cal}^\mathrm{m}$ = sampling point m on the calculated MWD under the lth set of operating conditions
$\overline{\mathrm{mwd}}\,(l)_\mathrm{tar}^\mathrm{m}$ = sampling point m on the target MWD under the lth set of operating conditions
n = polymer chain length ($n \geq 1$)
n_max = maximum chain length
N = number of data points
N_C = number of sets of operating conditions
N_P = number of sampling points on MWD curve
N_S = number of catalyst active sites
N_θ = number of estimated parameters
N_V = number of output variables under one set of operating conditions
P = reactor pressure, kPa
$P_0(j)$ = active site j of catalyst
$P_n(j)$ = living polymer chain of length n at site j
Q^U = rate of heat exchange in unit U, kJ/s
$\bar{R}$ = universal gas constant, 8.314 J/(mol·K)
$r_{C_\mathrm{d}(j)}$ = net reaction rate for deactivated site j of catalyst, mol/(L·s)
$r_{C_\mathrm{p}(j)}$ = net reaction rate for potential active site j of catalyst, mol/(L·s)
$r_{D_n(j)}$ = net reaction rate for dead chains of length n at site j, mol/(L·s)
$r_{P_0(j)}$ = net reaction rate for active site j of catalyst, mol/(L·s)
$r_{P_n(j)}$ = net reaction rate for living chains of length n at site j, j, mol/(L·s)
$r_{X^m(j)}$ = net reaction rate for mth moment of dead polymer at site j, mol/(L·s)
$r_{Y^m(j)}$ = net reaction rate for mth moment of living polymer at site j, mol/(L·s)
$r(\delta_i)$ = ratio of confidence interval δ_i to the corresponding kinetic parameter
$\mathrm{rsc}\,(k(j))$ = derivative of τ_j with respect to $k(j)$ in logarithmic form
θ = estimated parameter vector
θ^* = optimal estimated parameter vector
s = set of output variables in the estimation
$s(i,l)_\mathrm{cal}$ = ith calculated output variable under the lth set of operating conditions
$s(i,l)_\mathrm{tar}$ = ith target output variable under the lth set of operating conditions
T = reaction temperature, K
T_ref = reference temperature, K
$t_{\alpha/2}(N-N_\theta)$ = two-tails Student's t distribution with α confidence level, $N-N_\theta$ degrees of freedom
τ_j = ratio of all the chain transfer rates to the propagation rate

$\tau(l)_j^{\mathrm{cal}}$ = calculated τ at site j under the lth set of operating conditions
$\tau(l)_j^{\mathrm{tar}}$ = target τ at site j under the lth set of operating conditions
U = units: R(reactor), C(cooler), F(flash drum), and Comp (compressor)
V = reactor liquid volume, m^3
$w_{i,l}$ = weighting factor for the ith output variable under the lth set of operating conditions
$x_{\mathrm{CO}}^{\mathrm{U}}$ = liquid-phase mole fraction of component CO in unit U
$X^m(j)$ = mth moment of dead polymer at site j in the reactor, mol/L
$X_{\mathrm{in}}^m(j)$ = mth moment of dead polymer at site j fed into the reactor, mol/L
$y_{\mathrm{CO}}^{\mathrm{U}}$ = vapor-phase mole fraction of component CO in unit U
$Y^m(j)$ = mth moment of living polymer at site j in the reactor, mol/L
$Y_{\mathrm{in}}^m(j)$ = mth moment of living polymer at site j fed into the reactor, mol/L
$[.]$ = molar concentration of the inside component in the reactor, mol/L
$[.]_{\mathrm{in}}$ = molar concentration of the inside component fed into the reactor, mol/L
$[\mathrm{CO}]_{\mathrm{L}}^{\mathrm{U}}$ = liquid-phase molar concentration of component CO in unit U, mol/L
$[\mathrm{CO}]_{\mathrm{Lin}}^{\mathrm{U}}$ = liquid-phase molar concentration of component CO fed into unit U, mol/L
$[\mathrm{CO}]_{\mathrm{V}}^{\mathrm{U}}$ = vapor-phase molar concentration of component CO in unit U, mol/L
$[\mathrm{CO}]_{\mathrm{Vin}}^{\mathrm{U}}$ = vapor-phase molar concentration of component CO fed into unit U, mol/L
$\lfloor . \rfloor$ = operator rounding the argument down to the nearest integer

Literature Cited

1. Fontes CH, Mendes MJ. Analysis of an industrial continuous slurry reactor for ethylene-butene copolymerization. *Polymer*. 2005;46:2922–2932.
2. Soares JBP. Mathematical modelling of the microstructure of polyolefins made by coordination polymerization: a review. *Chem Eng Sci*. 2001;56:4131–4153.
3. Singh G, Kaur S, Naik DG, Gupta VK. Evolutionary computing approach for evaluating flory distribution curves in gel permeation chromatography: study of the poly(1-octene) system. *J Appl Polym Sci*. 2010;117:3379–3385.
4. Yoon WJ, Kim YS, Kim IS, Choi KY. Recent advances in polymer reaction engineering: modeling and control of polymer properties. *Korean J Chem Eng*. 2004;21:147–167.
5. Kou B, McAuley KB, Hsu CC, Bacon DW, Yao KZ. Mathematical model and parameter estimation for gas-phase ethylene homopolymerization with supported metallocene catalyst. *Ind Eng Chem Res*. 2005;44:2428–2442.
6. Matos V, Moreira M, Neto AGM, Nele M, Melo PA, Pinto JC. Method for quantitative evaluation of kinetic constants in olefin polymerizations, 3 kinetic study of the hiPP synthesis. *Macromol React Eng*. 2007;1:137–159.
7. Sirohi A, Choi KY. On-line parameter estimation in a continuous polymerization process. *Ind Eng Chem Res*. 1996;35:1332–1343.
8. Lo DP, Ray WH. Kinetic modeling and prediction of polymer properties for ethylene polymerization over nickel diimine catalysts. *Ind Eng Chem Res*. 2005;44:5932–5949.
9. Zavala VM, Biegler LT. Large-scale parameter estimation in low-density polyethylene tubular reactors. *Ind Eng Chem Res*. 2006;45:7867–7881.
10. Embiruçu M, Prata DM, Lima EL, Pinto PC. Continuous soluble Ziegler-Natta ethylene polymerizations in reactor trains, 2-estimation of kinetic parameters from industrial data. *Macromol React Eng*. 2008;2:142–160.
11. Li R, Corripio AB, Henson MA, Kurtz MJ. On-line state and parameter estimation of EPDM polymerization reactors using a hierarchical extended Kalman filter. *J Process Control*. 2004;14:837–852.
12. Khare NP, Seavey KC, Liu YA, Ramanathan S, Lingard S, Chen CC. Steady-state and dynamic modeling of commercial slurry high-density polyethylene (HDPE) processes. *Ind Eng Chem Res*. 2002;41:5601–5618.
13. Khare NP, Lucas B, Seavey KC, Liu YA, Sirohi A, Ramanathan S, Lingard S, Song Y, Chen CC. Steady-state and dynamic modeling of gas-phase polypropylene processes using stirred-bed reactors. *Ind Eng Chem Res*. 2004;43:884–900.
14. Thompson DE, McAuley KB, McLellan PJ. Parameter estimation in a simplified MWD model for HDPE produced by a Ziegler-Natta catalyst. *Macromol React Eng*. 2009;3:160–177.
15. Yao KZ, Shaw BM, Kou B, McAuley KB, Bacon DW. Modeling ethylene/butene copolymerization with multi-site catalysts: parameter estimability and experimental design. *Polym React Eng*. 2003;11:563–588.
16. Li R, Henson MA, Kurtz MJ. Selection of model parameters for off-line parameter estimation. *IEEE Trans Control Syst Technol*. 2004;12:402–412.
17. Embiruçu M, Lima EL, Pinto JC. Continuous soluble Ziegler-Natta ethylene polymerizations in reactor trains, 1-mathematical modeling. *J Appl Polym Sci*. 2000;77:1574–1590.
18. Embiruçu M, Pontes K, Lima EL, Pinto JC. Continuous soluble Ziegler-Natta ethylene polymerizations in reactor trains, 3-influence of operating conditions upon process performance. *Macromol React Eng*. 2008;2:161–175.
19. Fathi H, Schittkowski K, Hamielec AE. Dynamic modeling of living anionic solutionpolymerization of styrene/butadiene/divinylbenzene in a continuous stirred tank reactor train. *Polym Plast Technol*. 2004;43:571–613.
20. Weiss MER, Paulus F, Steinhilber D, Nikitin AN, Haag R, Schütte C. Estimating kinetic parameters for the spontaneous polymerization of glycidol at elevated temperatures. *Macromol Theory Simul*. 2012;21:470–481.
21. Gross J, Sadowski G. Perturbed-chain SAFT: an equation of state based on a perturbation theory for chain molecules. *Ind Eng Chem Res*. 2001;40:1244–1260.
22. Cressie N. The origins of kriging. *Math Geol*. 1990;22:239–252.
23. Zhang C, Zhan ZL, Shao ZJ, Zhao YH, Chen X, Gu XP, Yao Z, Feng LF, Biegler LT. Equation-oriented optimization on an industrial high-density polyethylene slurry process with target molecular weight distribution. *Ind Eng Chem Res*. 2013;52:7240–7251.
24. Zhan ZL. Simulation and optimization of an industrial HDPE slurry process based on equation-oriented models. M. Sc. Thesis, Zhejiang University, Hangzhou, China, 2012.
25. Soares JBP, Hamielec AE. Deconvolution of chain-length distributions of linear polymers made by multiple-site-type catalysts. *Polymer*. 1995;36:2257–2263.
26. Al-Saleh MA, Soares JBP, Duever TA. The integrated deconvolution estimation model: a parameter estimation method for ethylene/α-olefin copolymers made with multiple-site catalysts. *Macromol React Eng*. 2010;4:578–590.
27. Hakim S, Moballegh L. Simulation of a series of industrial slurry reactors for HDPE polymerization process using deconvolution of the GPC graph of only the first reactor. *Iran Polym J*. 2006;15:655–666.
28. Ray WH. On the mathematical modelling of polymerization reactors. *J Macromol Sci R M C*. 1972;8:1–56.
29. Dubé M, Soares JBP, Penlidis A, Hamielec AE. Mathematical modelling of multicomponent chain-growth polymerization in batch, semi-batch and continuous reactors. *Ind Eng Chem Res*. 1997;36:966–1015.
30. Flory PJ. *Principles of Polymer Chemistry*. New York: Cornell University Press, 1953.
31. Alghyamah AA, Soares JBP. Simultaneous deconvolution of the bivariate distribution of molecular weight and chemical composition of polyolefins made with Ziegler-Natta catalysts. *Macromol Rapid Commun*. 2009;30:384–393.
32. Lin WJ, Jacobson AM, Biegler LT. Modeling and optimization of a seeded suspension polymerization process. *Chem Eng Sci*. 2010;65:4350–4362.
33. Seber GAF, Wild CJ. *Nonlinear Regression*. New York: Wiley, 1989.
34. Marsili-Libelli S, Guerrizio S, Checchi N. Confidence regions of estimated parameters for ecological systems. *Econ Model*. 2003;165:127–146.
35. Zavala VM, Laird CD, Biegler LT. Interior-point decomposition approaches for parallel solution of large-scale nonlinear parameter estimation problems. *Chem Eng Sci*. 2008;63:4834–4845.

Appendix A: Unit Equation Models

Reactor

Mass Balance.

$$\left([\mathrm{M}]_{\mathrm{Lin}} * F_{\mathrm{Lin}}^{\mathrm{R}} + [\mathrm{M}]_{\mathrm{Vin}} * F_{\mathrm{Vin}}^{\mathrm{R}}\right) - \left([\mathrm{M}]_{\mathrm{L}} * F_{\mathrm{L}}^{\mathrm{R}} + [\mathrm{M}]_{\mathrm{V}} * F_{\mathrm{V}}^{\mathrm{R}}\right) = \sum_{j=1}^{Ns} \left(k_{\mathrm{i}}(j)[P_0(j)] + \left(k_{\mathrm{p}}(j) + k_{\mathrm{tM}}(j)\right) Y^0(j)\right) [\mathrm{M}]_{\mathrm{L}} * V \tag{A1}$$

$$([H_2]_{Lin} * F^R_{Lin} + [H_2]_{Vin} * F^R_{Vin}) - ([H_2]_L * F^R_L + [H_2]_V * F^R_V) = \sum_{j=1}^{Ns} k_{tH}(j)[H_2]_L^{0.5} Y^0(j) * V \tag{A2}$$

$$([C_6H_{14}]_{Lin} * F^R_{Lin} + [C_6H_{14}]_{Vin} * F^R_{Vin}) - ([C_6H_{14}]_L * F^R_L + [C_6H_{14}]_V * F^R_V) = 0 \tag{A3}$$

$$[A]_{in} * F^R_{Lin} - [A] * F^R_L = \sum_{j=1}^{Ns} (k_{aA}(j)[C_P(j)] + k_{tA}(j)Y^0(j))[A] * V \tag{A4}$$

$$[C_P(j)]_{in} * F^R_{Lin} - [C_P(j)] * F^R_L = -r_{C_p(j)} * V \tag{A5}$$

$$[C_d(j)]_{in} * F^R_{Lin} - [C_d(j)] * F^R_L = -r_{C_d(j)} * V \tag{A6}$$

$$[P_0(j)]_{in} * F^R_{Lin} - [P_0(j)] * F^R_L = -r_{P_0(j)} * V \tag{A7}$$

$$Y^0_{in}(j) * F^R_{Lin} - Y^0(j) * F^R_L = -r_{Y^0(j)} * V \tag{A8}$$

$$X^0_{in}(j) * F^R_{Lin} - X^0(j) * F^R_L = -r_{X^0(j)} * V \tag{A9}$$

$$Y^1_{in}(j) * F^R_{Lin} - Y^1(j) * F^R_L = -r_{Y^1(j)} * V \tag{A10}$$

$$X^1_{in}(j) * F^R_{Lin} - X^1(j) * F^R_L = -r_{X^1(j)} * V \tag{A11}$$

$$Y^2_{in}(j) * F^R_{Lin} - Y^2(j) * F^R_L = -r_{Y^2(j)} * V \tag{A12}$$

$$X^2_{in}(j) * F^R_{Lin} - X^2(j) * F^R_L = -r_{X^2(j)} * V \tag{A13}$$

Phase Equilibrium.

$$\varphi^R_{V,M} y^R_M = \varphi^R_{L,M} x^R_M \tag{A14}$$

$$\varphi^R_{V,H_2} y^R_{H_2} = \varphi^R_{L,H_2} x^R_{H_2} \tag{A15}$$

$$\varphi^R_{V,C_6H_{14}} y^R_{C_6H_{14}} = \varphi^R_{L,C_6H_{14}} x^R_{C_6H_{14}} \tag{A16}$$

Energy Balance.

$$(F^R_{Lin} C^R_{Lin} H^R_{Lin} + F^R_{Vin} C^R_{Vin} H^R_{Vin}) - (F^R_L C^R_L H^R_L + F^R_V C^R_V H^R_V) = -Q^R \tag{A17}$$

Polymer Property.

$$Mn = \frac{\sum_{j=1}^{Ns} (Y^1(j) + X^1(j))}{\sum_{j=1}^{Ns} (Y^0(j) + X^0(j))} * mw \tag{A18}$$

$$Mw = \frac{\sum_{j=1}^{Ns} (Y^2(j) + X^2(j))}{\sum_{j=1}^{Ns} (Y^1(j) + X^1(j))} * mw \tag{A19}$$

$$PDI = \frac{Mw}{Mn} \tag{A20}$$

Cooler

Mass Balance.

$$[M]^C_{Vin} * F^C_{Vin} - ([M]^C_L * F^C_L + [M]^C_V * F^C_V) = 0 \tag{A21}$$

$$[H_2]^C_{Vin} * F^C_{Vin} - ([H_2]^C_L * F^C_L + [H_2]^C_V * F^C_V) = 0 \tag{A22}$$

$$[C_6H_{14}]^C_{Vin} * F^C_{Vin} - ([C_6H_{14}]^C_L * F^C_L + [C_6H_{14}]^C_V * F^C_V) = 0 \tag{A23}$$

Phase Equilibrium.

$$\varphi^C_{V,M} y^C_M = \varphi^C_{L,M} x^C_M \tag{A24}$$

$$\varphi^C_{V,H_2} y^C_{H_2} = \varphi^C_{L,H_2} x^C_{H_2} \tag{A25}$$

$$\varphi^C_{V,C_6H_{14}} y^C_{C_6H_{14}} = \varphi^C_{L,C_6H_{14}} x^C_{C_6H_{14}} \tag{A26}$$

Energy Balance.

$$F^C_{Vin} C^C_{Vin} H^C_{Vin} - (F^C_L C^C_L H^C_L + F^C_V C^C_V H^C_V) = -Q^C \tag{A27}$$

Flash drum

Mass Balance.

$$([M]^F_{Lin} * F^F_{Lin} + [M]^F_{Vin} * F^F_{Vin}) - ([M]^F_L * F^F_L + [M]^F_V * F^F_V) = 0 \tag{A28}$$

$$([H_2]^F_{Lin} * F^F_{Lin} + [H_2]^F_{Vin} * F^F_{Vin}) - ([H_2]^F_L * F^F_L + [H_2]^F_V * F^F_V) = 0 \tag{A29}$$

$$([C_6H_{14}]^F_{Lin} * F^F_{Lin} + [C_6H_{14}]^F_{Vin} * F^F_{Vin}) - ([C_6H_{14}]^F_L * F^F_L + [C_6H_{14}]^F_V * F^F_V) = 0 \tag{A30}$$

Phase Equilibrium.

$$\varphi^F_{V,M} y^F_M = \varphi^F_{L,M} x^F_M \tag{A31}$$

$$\varphi^F_{V,H_2} y^F_{H_2} = \varphi^F_{L,H_2} x^F_{H_2} \tag{A32}$$

$$\varphi^F_{V,C_6H_{14}} y^F_{C_6H_{14}} = \varphi^F_{L,C_6H_{14}} x^F_{C_6H_{14}} \tag{A33}$$

Energy Balance.

$$(F^F_{Lin} C^F_{Lin} H^F_{Lin} + F^F_{Vin} C^F_{Vin} H^F_{Vin}) - (F^F_L C^F_L H^F_L + F^F_V C^F_V H^F_V) = -Q^F \tag{A34}$$

Compressor (isentropic compression)

Mass Balance.

$$[M]^{Comp}_{Vin} * F^{Comp}_{Vin} - [M]^{Comp}_V * F^{Comp}_V = 0 \tag{A35}$$

$$[H_2]^{Comp}_{Vin} * F^{Comp}_{Vin} - [H_2]^{Comp}_V * F^{Comp}_V = 0 \tag{A36}$$

$$[C_6H_{14}]^{Comp}_{Vin} * F^{Comp}_{Vin} - [C_6H_{14}]^{Comp}_V * F^{Comp}_V = 0 \tag{A37}$$

Energy Balance.

$$E_f = \frac{H^{Comp}_S - H^{Comp}_{Vin}}{H^{Comp}_V - H^{Comp}_{Vin}} \tag{A38}$$

Appendix B: Proof of Mole Fraction Equality

Despite different sets of reactor operating conditions in the steady-state HDPE slurry process, we observe that mole fractions of the polymer produced at the same site j are almost the same. To justify and analyze this observation, we first make the following reasonable assumptions:

1. The concentrations of the active site $[P_0(j)]$ and the living polymer chain of unit length $[P_1(j)]$ in the reactor are negligible.
2. The values of the transfer-to-monomer rate constant $k_{tM}(j)$ are negligible when compared with the values of the propagation rate constant $k_p(j)$.

3. The values of the activation energy of the propagation reaction $E_p^a(j)$ are equal at each site, so are the concentration of the potential active site $[C_p(j)]$, and the activation and deactivation rate constant $k_{aA}(j)$ and $k_d(j)$.

Equations A7, A8, A10, and A11 are the steady-state population balances of $P_0(j)$, $Y^0(j)$, $Y^1(j)$, $X^1(j)$. $[P_0(j)]_{in}$, $Y^0_{in}(j)$, $Y^1_{in}(j)$, $X^1_{in}(j)$ are the corresponding molar concentrations at the jth active site in the total feed flow. For the first reactor, $[P_0(j)]_{in}$, $Y^0_{in}(j)$, $Y^1_{in}(j)$, $X^1_{in}(j)$ are all zero. Adding Eqs. A10 and A11 together and simplifying the resulting expression

$$Y^1(j)+X^1(j)=\left(\begin{array}{l} k_p(j)[M]_L^R Y^0(j)+k_{tM}(j)[M]_L^R Y^0(j) \\ \\ +k_i(j)[M]_L^R[P_0(j)]-k_{tM}[M]_L^R[P_1(j)] \end{array}\right)*V/F_L^R \cong k_p(j)[M]_L^R Y^0(j)*V/F_L^R \tag{B1}$$

Adding Eqs. A7 and A8 together and simplifying the resulting expression, one obtains

$$Y^0(j)=k_{aA}(j)\left[C_p(j)\right][A]*V/\left(F_L^R+k_d(j)V\right)-[P_0(j)] \cong k_{aA}(j)\left[C_p(j)\right][A]*V/\left(F_L^R+k_d(j)V\right) \tag{B2}$$

Substituting Eq. B2, Eq. B1 becomes

$$Y^1(j)+X^1(j) \cong k_p(j)k_{aA}(j)\left[C_p(j)\right][M]_L^R[A] *V^2/\left(F_L^R\left(F_L^R+k_d(j)V\right)\right) \tag{B3}$$

Because the values of $k_{aA}(j)$, $k_d(j)$, and $[C_P(j)]$ are equal at all active sites, substituting Eqs. 1 and B3 into Eq. 23, one obtains

$$mf_j=\frac{Y^1(j)+X^1(j)}{\sum_{j=1}^{Ns}\left(Y^1(j)+X^1(j)\right)} \cong \frac{k_p(j)}{\sum_{j=1}^{Ns}k_p(j)}=\frac{k_p^0(j)}{\sum_{j=1}^{Ns}k_p^0(j)} \tag{B4}$$

Similar equations can be derived for the mf_j in the second reactor.

Manuscript received Dec. 13, 2013, and revision received June 6, 2014.